Biologically effective daily radiant exposure for erythema appearance, previtamin D_3 synthesis and clearing of psoriatic lesions derived from ~~erythema biometers~~erythemal broadband meters at Belsk, Poland, for the period 1976-2023

Janusz W. Krzyścin[1], Agnieszka Czerwińska[1], Bonawentura Rajewska-Więch[1], Janusz Jarosławski[1], Piotr S. Sobolewski[1], Izabela Pawlak[1]

~~1Institute~~1 Institute of Geophysics, Polish Academy of Sciences, Warsaw, 01-452, Poland

Correspondence to: Janusz W. Krzyścin (jkrzys@igf.edu.pl)

Abstract. A long-term series of exposures to solar ultraviolet ~~(UV)~~ radiation (UVR) is required to assess the risks and benefits of radiation on different human biological processes. However, homogenisation of the amount of biologically effective solar energy ~~reaching the Earth's surface over long periods (i.e.~~(i.e. energy weighted according to the sensitivity of the selected biological process to solar radiation) reaching the Earth's surface over long periods is challenging due to changes in measurement methods and instruments. This paper presents the world's longest homogenised time series of biologically effective daily radiant exposures (DRE) from regular monitoring with different erythemal ~~biometers (EB~~broadband radiometers (EBRs) operated at the Central Geophysical Laboratory of the Institute of Geophysics, Polish Academy of Sciences (IG PAS), Belsk (20.79°E, 51.84°N) from 1 January 1976 to 31 December 2023. The following biological effects were considered: the ~~appearance of~~ erythema, cutaneous synthesis of previtamin D_3, and clearing of psoriatic lesions. The data for the latter two biological effects are estimated based on the proposed method of using ~~EB~~EBR measurements to calculate other non-erythemal DRE. The following ~~broadband erythemal radiometers~~EBRs were used in the monitoring: Robertson-Berger (1975−1992), Solar Light model 501 (1993−1994 with #927, 1995−2013 with #2011) and Kipp-Zonen UV-AE-T #30616 from 5 August 2013 to the present. From 1976 to 2013, the homogenisation procedure consisted of comparing the measured erythemal DRE and daily maximum of UV index (~~erythemal irradiance at noon~~UVI_{MAX}) with the corresponding synthetic values from simulations using a radiation transfer model~~.~~ for cloudless conditions. Between 2014 and 2023, the ~~raw~~EBR data were compared with data from a collocated reference instrument, the Brewer Mark II #64 spectrometer. Such comparisons resulted in a set of multipliers that were applied to the ~~raw EB~~EBR measurements. Two different versions of the homogenisation method were applied ~~(~~analysing modelled and observed values for erythemal DRE and ~~UV index with~~UVI_{MAX} assuming different ~~selection of~~criteria for cloudless days~~), and three~~. Three regression models ~~were constructed for~~ of the erythemal data ~~based~~ on common UVR indices (total column ozone, aerosol optical depth and global clear sky irradiance ~~clearness index.~~index) were used to reconstruct the UVR data from the beginning of the Belsk observations, allowing further validation of the homogenised UVR data. Linear trends calculated ~~from reevaluated and reconstructed time series (a total of seven time series were considered)~~ showed a statistically significant increase in erythemal annual and summer (June to August) radiant exposures of about 6 % per decade over the period 1976−2005. Thereafter, no trend was observed. The same trend estimates were found for all biological effects considered.

The ~~raw and reevaluated~~ data are made freely available via the following repository: https://doi.org/10.1594/PANGAEA.972139 (Krzyścin et al., 2024). An additional version of the ~~reevaluated~~re-evaluated data, together with the corresponding clear sky and proxy data used in the ~~UV~~UVR data reconstruction, is archived at: https://doi.org/10.25171/InstGeoph_PAS_IGData_Biologically_Effective_Solar_Radiation_Belsk_1976_2023 (Krzyścin, 2024).

Keyword(s): ~~biometer~~erythemal broadband radiometer; biologically effective irradiance, homogenisation, radiant exposure

1 Introduction

Molina and Rowland (1974), winners of the 1995 Nobel Prize in Chemistry, argued that man-made chlorofluorocarbons (CFCs), which were widely used in industry in the 1970s, could ~~penetrate~~reach the stratospheric ozone layer where they ~~were~~would be destroyed by short-wave ultraviolet ~~(UV)~~ radiation~~,~~ (UVR), releasing free chlorine atoms and causing stratospheric O_3 depletion in the catalytic reaction cycle. Solar radiation in the shortest part of its spectrum that reaches the Earth's surface (290−315 nm), known as UV-B, is strongly absorbed by stratospheric ozone. The discovery of the ozone hole over Antarctica (Chubachi, 1984; Farman et al., 1985) and the predicted decreasing trend in total column ozone (TCO_3) in other regions have stimulated interest in establishing continuous monitoring of UV-B irradiance reaching the ground. In addition, there is growing evidence that such ~~UV~~UVR trends can cause various adverse health effects, such as skin cancers (including the deadly melanoma), DNA damage, immunosuppression, oxidative stress and skin ageing (Neale et al., 2023).

Solar UV-B radiation from space is attenuated as it passes through the atmosphere due to light scattering (by cloud particles, atmospheric gases and aerosols) and absorption (by O_3, NO_2, SO_2 and aerosols). The attenuation of light increases with its path length through the atmosphere (i.e. usually described by the air mass), so solar elevation and ground surface altitude are key parameters to consider in surface ~~UV~~UVR modelling. Other factors forcing ~~UV~~UVR variability at the surface that are often used as proxies for atmospheric UV-B attenuation are total column O_3 (TCO_3) to account for ~~UV~~UVR absorption by ozone, the ~~clearness~~clear sky index (CI) (i.e. a quotient of the all-sky global solar irradiance (~~GSI~~G) at the surface and the corresponding synthetic clear-sky value (G_0) to account for combined cloud/aerosol scattering effects on ~~UV~~UVR), and aerosol optical depth (AOD) in the solar UV range (parameterising ~~UV~~UVR attenuation by aerosols). TCO_3 and ~~GSI~~G have been found to be the most effective for modelling surface UV-B radiation (Koepke et al., 2006, den Outer et al., 2010).

In the early 1970s, the broadband Robertson-Berger (RB) meter was developed to measure the biologically effective (BE) ~~UV radiation~~UVR that causes skin redness, also known as erythema (Berger, 1976). The spectral characteristics of RB resembled the erythemal sensitivity of human skin. RB instruments began continuous monitoring of erythemal irradiance in 1974 at eight sites in the United States (Scotto et al., 1988). During the 1970s, instruments were operated in other countries (Austria, Australia, Germany, Poland, Sweden, Switzerland) (WMO, 1977). At the beginning of this global network, RB meters were calibrated using a travelling standard meter provided by the Photobiology Center at Philadelphia University. After a few years, at some stations, including the Institute of Geophysics, Polish Academy of Sciences (IG PAS) station at Belsk (51.84°N, 20.78°E), this calibration method was replaced by comparisons with values modelled by the radiative transfer model. The Dave-Halpern model (Dave and Halpern, 1976) was used to estimate erythemally weighted irradiance for cloudless

sky conditions to calibrate the Belsk data (Słomka and Słomka, 1985). Serious drawbacks of RB measurements were their results in relative units (counts), temperature sensitivity, a lot of manual work in data preparation, sometimes rapid ageing, and difficulties in accurately converting counts into the so-called sunburn unit (the minimum erythemal radiation exposure that causes redness of the skin). These problems were significantly reduced in a new version of the RB meter, a prototype of the current ~~UV biometer,~~erythemal broadband radiometer (EBR), developed in the late 1980s as a result of collaboration between IG PAS and the Institute of Medical Physics of the University of Innsbruck (Blumthaler et al., 1989; Słomka and Słomka, 1993). Further prototype work at Solar Light (SL) Co. in Philadelphia resulted in the production of a commercial SL Biometer ~~Mod~~Model 501A, which replaced the RB meter.

Other EBR versions ~~of broadband UV biometers for UV monitoring~~ were introduced in the 1990s, including those from Yankee Environmental Systems (Turner Falls, USA) and Kipp and Zonen (KZ) Co. (Delf, Netherlands). However, there was a need to standardise the ~~calibration~~correction procedure for the broadband ~~UV~~UVR meters as it became apparent that the calibration provided by the manufacturer could not be relied upon even for the same type of instrument (Leszczynski et al., 1998). A standard calibration method that takes into account the individual spectral characteristics of the instrument and the loss of sensitivity has been proposed (Hülsen and Gröbner 2007). However, uncertainties of ~7 % can still be expected for well-maintained ~~biometers~~EBRs (Gröbner et al., 2009).

Long-term series of surface UVR from ground-based observations with a length of at least a few decades are rare. To the authors' knowledge, the longest UVR monitoring series began in Moscow in 1968 with a broadband (300−380 nm) instrument developed at the Moscow State University Meteorological Observatory (Chubarova et al., 2000). One of the world's longest measurements of solar UVR at the Earth's surface (and probably the longest taken by erythemal broadband instruments) are from Belsk. Measurements began in 1975 and continuous monitoring started on 1 January 1976. From a global perspective, the first UVR results appeared at the World Ozone and Radiation Data Centre (WOUDC) in 1989, but continuous UVR time series over three decades are only available for a limited number of stations including: Uccle (Belgium), Edmonton, Resolute, Toronto, Churchill, Saturna Island (Canada), Tateno (Japan) and Syowa (Antarctica) (WOUDC, 2025). Database Network for the Detection of Atmospheric Composition Change (NDACC) include also stations with at least of three decades of UVR measurements such as Lauder (New Zealand), Mauna Loa (USA) and three Antarctica stations – Arrival Heights, Palmer Station and South-Pole (NDACC, 2025).

This article presents a retrospective evaluation of all ~~UV~~UVR measurements (1976−2023) at Belsk made with different ~~broadband instruments~~EBRs including: RB (1976–1992), SL ~~biometer~~Biometer model 501 A (SL501 A) (two instruments were used #927 and #2011 for the period 1993−1994 and 1995−2013, respectively) and KZ UV-AE-T #30616 (KZ616) from 5 August 2013 to the present. The ~~reevaluation~~re-evaluation for the period 1976−2013 is based on a comparison of the measurements with the synthetic daily erythemal ~~irradiance~~radiant exposure and UV index ~~(the midday value of erythemal irradiance)~~at noon from a radiative model simulation for clear sky conditions using TCO_3 and AOD measured at Belsk as model input parameters. The quality of the KZ616 data (2013−2023) will be accessed through comparisons with clear-sky erythemal irradiances simultaneously measured by the well-maintained Brewer spectrophotometer Mark II #64 (BS64). The details of the Brewer maintenance can be found in Czerwińska and Krzyścin (2024a). Erythemal daily radiant exposures (DRE) for the entire period of the ~~UV~~UVR measurements at Belsk will be transferred to the corresponding vitamin D_3 and antipsoriatic DRE using a method proposed by Czerwińska and Krzyścin (2024a). A comparison of these DRE with those from BS64

spectral measurements in the period 2014-2023 will indicate the accuracy of the proposed reconstruction method of past BE data based on a statistical approach using typical proxies (TCO_3, ~~GSI~~ and G) characterising atmospheric ~~UV~~UVR attenuation. Finally, trend calculations in annual (January–December) and summer (June–August) radiant exposures (RE) for all biological effects considered and versions of the recalculated ~~UV~~UVR data from 1976–2023 will be presented to confirm the robustness of the long-term changes in the BE radiation measured at Belsk.

2 Materials and Method

2.1 ~~UV~~UVR monitoring

~~The recording~~Recording of ~~solar erythemal~~erythema irradiance with a standard RB meter (detector recorder #No. 40~~), initiated in Belsk~~) started in May 1975~~, was carried out~~ at Belsk, but continuous monitoring began on 1 January 1976 and lasted until 1994. From May 1993, in parallel with the RB measurements, the monitoring of erythemal irradiance using the SL Biometer 501 A #927 was initiated in order to establish monthly transfer coefficients for converting the RB output in sunburn units (SU) into erythemal units, i.e. the minimum erythemal dose (MED) causing skin redness in typical Caucasian skin, which was entered into the SL Biometer 501 A measurements (Puchalski, 1995). It was assumed that 1 MED~~=~~ = 210 J_{eryt} m^{-2}, where J_{eryt} denotes spectral irradiance integrated over time and wavelengths (290–400 nm) after weighting by the erythema action spectrum~~ (CIE, 2019).~~. Simultaneous measurements continued until December 1994, and all erythemal DRE measured with the RB meter before 1993 were multiplied by these transfer coefficients to obtain data comparable to those with the SL Biometer 501 A.

As the RB meter showed sensitivity to ambient temperature, a correction for temperature effect was applied to the raw daily RB values (Borkowski, 1998) using empirical formulas proposed by Koskela et al. (1994). In addition, the RB Belsk series was also found to be affected by a change in calibration method in 1985, as the Dave-Halpern model (Dave and Halpern, 1976) calculations for cloudless conditions replaced field comparisons with the travelling standard instrument. This resulted in a downward step change of 14 % in the ~~UV~~UVR series (Borkowski, 2000). The ~~recevaluated~~re-evaluated time series of erythemal DRE for the period 1976–1992 as made by Borkowski (2008) was archived and formed part of the ~~raw~~ Belsk's erythemal time series (1976–2023), which is further homogenised in this study.

Subsequent ~~UV~~UVR measurements included SL501 A # 927 (1993–1994) and #2011 (1995–2013), which were only ~~pre~~ roughly calibrated by the instrument manufacturer~~.~~ prior to shipment. In 2005, KZ616 was added to the IG PAS UV network and served as the reference instrument. It was not used for everyday ~~UV~~UVR monitoring but only for occasional international calibration campaigns to provide a source for further calibrations with our SL biometers operating in Belsk and Hornsund (Spitzbergen). KZ616 started regular ~~UV~~UVR monitoring on 5 August 2013, replacing the ~~previous~~raw SL501 A #2011, as BS64 (normally measuring TCO_3 and Umkehr ozone at Belsk since 1992) was established as the new ~~UV~~UVR reference instrument for the IG PAS network, which has been in operation until now. The performance of KZ616 has ~~proved~~proven to be very stable and it is still involved in regular ~~UV~~UVR monitoring.

In the following, we use the term "raw data" for the results of the EBR measurements in W m^{-2} and J m^{-2} that were previously archived in the internal databases of IG PAS before the release of the Krzyścin et al. (2024) and Krzyścin (2024) databases.

2.2 Ancillary data

Daily representatives of TCO_3 at Belsk are taken from the IG PAS data portal (Krzyścin, 2024), which contains results of daily average TCO_3 measurements throughout the day, prepared for ~~UV~~UVR modelling purposes. For example, the most reliable daily representative value of TCO_3 (marked with flag no. 1) was calculated as an average of the most accurate measurements (the so-called direct sun measurements) made by the Dobson spectrophotometer between 9:00 and 13:00 UTC. The least accurate case of ground-based TCO_3 observations (with flag no. 5) occurred under cloudy and low sun elevation conditions, i.e. before 9:00 and after 13:00 UTC. In this case, only the least reliable Dobson observations were available for calculating the daily TCO_3 representative under overcast zenith and high air masses. In the rare cases when ground observations were not available, satellite data (flag 6 or 7 depending on the data source) and/or TCO_3 reanalysis data (flag 8) were used.

The daily representative of CI, DCI, which is ~~a commonly~~further used ~~measure of cloud attenuation of global (direct and diffuse) solar irradiance at ground level (Liu and Jordan, 1960). Daily values of CI are~~ in regression models (Sect. 2.3.4), is calculated as the quotient of the ~~all-sky (G) and the corresponding synthetic clear-sky (~~daily integrals (sunrise to sunset) of G and G_0~~) daily integral of global solar irradiance.~~. Typically, ~~G is derived from observations and G_0 from a model simulation, depending on the amount of solar absorbers (mostly water vapour) and AOD. Global solar DRE~~ the former values were obtained from routine monitoring of global solar irradiance by various pyranometers (since 1965) including the following instruments: Kipp & Zonen CM 6, Sonntag PRM-2, Kipp & Zonen CM 5, Kipp & Zonen CM 11, and Kipp & Zonen CM 21. The data were calibrated using the Polish national standard, which ~~was~~had previously ~~calibrated~~been adjusted to the world standard during inter-comparison campaigns at the World Radiation Centre in Davos, Switzerland. In addition, the Campbell-Stokes sunshine recorder provided the duration of sunshine per day to pre-select sunny days. All these data are archived in the IG PAS Data Portal (Krzyścin, 2024).

To ~~support~~validate the ~~quality of the~~corrected UV observations at Belsk, the long-term variability of BE ~~radiance~~radiation was also obtained from the ~~UV~~UVR reconstruction models (Section 2.3) using proxies (TCO_3 and ~~CI~~DCI) from the ground-based observations and reanalysis datasets. The European Centre for Medium-Range Weather Forecasts (ECMWF) v5 (ERA5) reanalysis provides, in addition to many other variables, intra-day TCO_3 values, ~~global solar irradiance for clear sky~~G_0, and ~~all−sky conditions~~G for the period 1940−2024, which are freely available on the ERA5 (~~2024~~2025) website. Also included are data (from 1 January 1980 to the present) downloaded from the Modern-Era Retrospective Analysis for Research and Applications version 2 (MERRA-2) database (GMAO, ~~2024~~2025) using the Giovanni data search tool, which is freely available on the Giovanni (~~2024~~2025) website.

Table 1. The Belsk's instruments and their working periods.

Data	Instrument/data	Operation period	Reference
Daily ERE and UV Index	Robertson Berger Meter	1976−1994	Krzyścin et al. (2024)
	SL Biometer 501 A # 927	1992−1994	
	SL Biometer 501 A # 2011	1995−2013	Krzyścin (2024)
	Kipp-Zonen UV-AE-T # 30616	2013−present	
TCO_3	Dobson Spectrophotometer # 84	1963−present	Krzyścin (2024)
SunDur	Campbell–Stokes sunshine recorder	1966−1968, 1970−1973, 1975−present	Krzyścin (2024)
G	Kipp CM 6	1965−1980	Krzyścin (2024)
	Sonntag PRM-2	1981−1987	

	Kipp&Zonen CM 5	1988−1991	
	Kipp&Zonen CM 11	1992−2010	
	Kipp&Zonen CM 21	2010−present	
AOD_{340nm}	Sonntag pyrheliometers	1976−2013	Krzyścin (2024)
	CIMEL CE 318-T	2004−present	
G and G_0	ERA5 reanalysis	1940−present	ERA5 (2025)
G_0	MERRA-2 reanalysis	1980−present	GMAO (2025)

Atmospheric aerosols can be significant drivers of surface ~~UV radiation~~UVR, especially under clear sky conditions (Krzyścin and Puchalski, 1998). The column properties of aerosols can be obtained from ground-based observations and used in the modelling of radiative transfer in the atmosphere. Aerosol properties are described by various characteristics (e.g. including AOD, single scattering albedo, asymmetry factor). In this article, we use Belsk's AOD at 340 nm (IG PAS Data Portal, Krzyścin (2024)), which is estimated from the Linke turbidity factor measurements with Sonntag pyrheliometers between 1976 and 2013 (Posyniak et al., 2016) and from the co-located solar photometer CIMEL CE 318-T (~~2014~~2004−2023) operating within the Aerosol Robotic Network (AERONET) (AERONET, ~~2024~~2025). Other aerosol properties are kept constant and equal to their typical values for the rural site. Table 1 summarises the sources of the data used in this paper.

2.3 ~~UV~~UVR models

2.3.1 Clear-sky model

Radiative transfer model simulations for clear sky conditions are used to quantify and correct biases in the output of the Belsk UVR radiometers. To speed up the calculations, the look-up tables were obtained using the Tropospheric Ultraviolet and Visible (TUV) Radiative Transfer Model (TUV, 2025).

Synthetic clear-sky values of BE (erythema ~~appearance~~, previtamin D_3 synthesis, clearing of psoriasis lesions) RE ~~and~~ in day D, $RE_{EFF,CS}(D)$ in J_{EFF} m^{-2}, and irradiance at noon ~~in day D, $RE_{EFF,CS}(D)$ in J_{eff} m^{-2}, and~~ $Ir_{EFF,CS}(t{=}\text{noon})$, in ~~$W_{eff}$~~$W_{EFF}$ m^{-2}, respectively, are ~~derived from look-up tables obtained from the Tropospheric Ultraviolet and Visible (TUV) radiation transfer model (TUV, 2024);~~calculated using the following formulas:

$$RE_{EFF,\ CS}(D) = \int_{Sunrise(D)}^{Sunset(D)} Ir_{EFF,\ CS}(t)dt \quad (1)$$

$$Ir_{EFF,\ CS}(t) = \int_{290\ \text{nm}}^{400\ \text{nm}} Ir_{CS}(\lambda, t)\ AS_{EFF}(\lambda)d\lambda \quad (2)$$

where ~~$Ir(\lambda, t)$~~ $Ir_{CS}(\lambda, t)$ is the spectral irradiance ~~in~~at time t ~~for the~~and at wavelength λ, and $AS_{\mathrm{EFF}}(\lambda)$ denotes the action spectrum for specific biological effect EFF: EFF=ERYT for erythema (CIE 2019), EFF=VITD3 for photosynthesis of previtamin D_3 in human skin (CIE 2006), and EFF=PSOR for psoriasis clearing (Krzyścin et al., 2012). Figure 1 presents the action spectra used.

Figure 1. Normalised action spectra for the specific biological effects: erythema ~~appearance,~~(eryt), photosynthesis of previtamin D_3 in human skin~~,~~ (vitD3), psoriasis clearing~~.~~ (psor).

Input to the clear-sky version of TUV model (daily representatives of TCO_3, annual and monthly mean AOD at 340 nm for the period 1976−2013 and 2014−2023, respectively) and output (~~$RE_{EFF,Clear-Sky}(D)$ and $Ir_{EFF,Clear-Sky}RE_{EFF,CS}(D)$~~ and $Ir_{EFF,CS}(t$=noon), where EFF={ERYT, VITD3, PSOR}), are archived in IG PAS Data Portal (Krzyścin, 2024).

2.3.2 ~~Reevaluation~~Re-evaluation of the ~~UV~~UVR measurements

Model simulations of erythemal DRE and noon UVI under cloudless sky provide a basis for the correction procedure of the past UVR data. A selection of clear-sky conditions throughout the entire day from the daily proxy values (relative sunshine duration and DCI), which were available for Belsk, is not straightforward as only the examination of the daily course of these measurements would allow to capture cloudless moments within the day. Thus, two different sets of correction coefficients are proposed, called CC1 and CC2.

The intraday ~~UV~~UVR measurements at Belsk from 1976 to 2023 can be clearly divided into three periods:

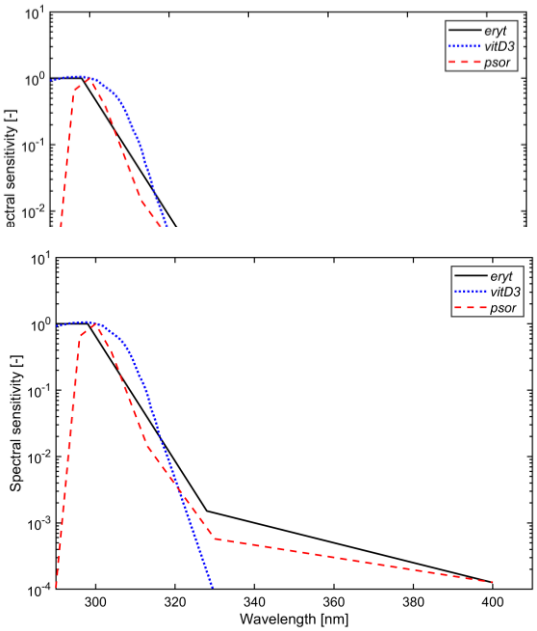

1 January 1976−31 December 1992, 1 January 1993−4 August 2013, and 5 August 2013−31 December 2023, according to the different broadband instruments used for ~~UV~~UVR monitoring, i.e. RB, SL501 A, and KZ616, respectively. For the first period, only the ~~daily~~ erythemal ~~RE was~~DRE were archived, whereas for other periods ~~the erythemal irradiances at noon, the so called~~daily maximum of UV index (~~UVI), were~~UVI_{MAX}) was also available~~.~~ (equal to the value of erythemal irradiance at noon during a cloudless day). There were also periods when both instruments were operated simultaneously for calibration purposes: March 1992−December 1994 (RB

versus SL501 A), 5 August 2013−31 December 2014 (SL501 A #2011 versus KZ616), and 5 August 2013−31 December 2023 (KZ616 versus BS64).

The ~~calibration~~correction procedure before 5 August 2013 consisted of comparing the raw erythemal data with the corresponding synthetic values obtained from the radiative model simulations (described in Sections 2.3.1) for ~~the~~ days when ~~clear sky conditions can be assumed from the~~ ancillary data~~.~~ indicated that the sky was clear throughout the day. The ~~locally weighted scatterplot smoother~~LOcally Weighted Scatterplot Smoothing (LOWESS~~,~~) proposed by Cleveland~~,~~ (1979) was used to extract the smoothed pattern of the multipliers of the raw ~~UV~~UVR data, i.e. the ~~calibration~~correction coefficients (CCs), from the daily ratios between synthetic and erythemal REs (for version CC1 of the ~~calibration~~correction) or from the ratios between ~~UVIs~~UVI_{MAX} (version CC2~~) taken for the days when clear sky conditions can be assumed at Belsk. Two sets of CCs were examined to determine the range of uncertainty in the CC estimates. In order to allow for greater variability in the CC values, different criteria for clear sky conditions were applied, and the smoothing procedure was applied to the long (1976−2013) and short (1993−2013) UV time series for the CC1 and CC2 versions, respectively. Accordingly, the~~). The following conditions were applied for the selection of clear sky ~~sets:~~data used in the two correction methods:

- CC1 – direct sun TCO_3 measurements occurred between 9:00−13:00 UTC (code 1 for the TCO_3 observation in IG PAS Data Portal, Krzyścin (2024)) and the daily difference between the observed and the theoretical maximum sunshine duration ~~and theoretical one (for SZA < 85°)~~ is less than ~~0.5 hour as for higher SZA broad band UV~~30 minutes at solar zenith angles (SZAs) below 85°. This limit was chosen because broadband UVR measurements at larger SZAs are unreliable and the Campbell-Stokes instruments starts when direct sun irradiance exceeded 120 W m^{-2}.
- CC2 – ~~For~~for TCO_3, the same condition was set as for CC1, and the ratio between the observed and theoretical sunshine hours (for SZA < 85°) is not less than 85 %. CC2 values have only been calculated for the period since 1 January 1993. ~~Prior to this date, we assumed that the calibration coefficients were equal to 1.0 according to the recalibration of the RB data in 2011 (Krzyścin et al., 2011).~~Prior to this date, a re-evaluation of the RB data with a model mimicking the KZ radiometer measurements by Krzyścin et al. (2011) showed that the correction was not necessary, i.e. CC2=1. This choice is also confirmed here by the constant long-term patterns of CC1 in the period 1976-1992 (Fig. 6a), and only a small jump in the differences between CC1 and CC2 in 1992/1993 (Fig. 6b)

Different criteria for the selection of cloudless days would result in even greater differences between the two CC versions. In addition, the smoothing procedure was applied to the long (1976-2013) and short (1993-2013) UVR time series for the CC1 and CC2 versions, respectively. We would like to have two different sets of correction coefficients to find out how the long-term pattern of biologically effective radiation is sensitive to the corrections. The CC1 and CC2 versions of the ~~reevaluated~~re-evaluated Belsk ~~UV~~UVR data are stored in the following free-access data archives: https://doi.org/10.1594/PANGAEA.972139 (Krzyścin et al., 2024) and https://doi.org/10.25171/InstGeoph_PAS_IGData_Biologically_Effective_Solar_Radiation_Belsk_1976_2023 (Krzyścin, 2024), respectively.

2.3.3 Reconstruction of BE radiation from the erythemal data

Broad-band instruments for measurement of the erythemal irradiance can also estimate non-erythemal irradiance by multiplying the erythemal irradiance by the so-called conversion factors (CF_{EFF}) derived from spectral ~~UV~~UVR measurements and/or radiative transfer simulations (Schmalwieser et al., 2022; Czerwińska and Krzyścin, 2024a):

$$Ir_{EFF}(t) = CF_{EFF}\,(TCO_3, SZA) \times Ir_{ERYT}(t), \quad (3)$$

where SZA denotes the solar zenith angle at time t. Following this concept, the daily radiant exposure for previtamin D_3 synthesis and psoriasis clearance ~~on the current D~~ in year (YR), month (MM), and day~~,~~ of month (DD) RE_{VITD3}~~(D)~~(YR, MM, DD) and RE_{PSOR}~~(D)~~,(YR, MM, DD), respectively, were estimated using the daily conversion factor, CF^*_{EFF}, applied to the ~~recevaluated~~ erythemal DRE~~:~~ ($RE_{ERYT}(YR, MM, DD)$):

$$RE_{EFF}\text{~~}(D)\text{~~}(YR, MM, DD) = CF^*_{EFF}\text{~~}(TCO_3, D^*) \times RE_{ERYT}\text{~~}(D)\text{~~}(TCO_3, JD\,) \times RE_{ERYT}(YR, MM, DD),\ EFF = \{VITD3, PSOR\}, \quad (4)$$

where CF^*_{EFF} depends on TCO_3 and ~~D^*~~JD (Julian day ~~of the year (i.e. between 1 and 365/366)~~number corresponding to the current ~~D~~ day~~.~~ {YR, MM, DD}). CF^*_{EFF} and CF_{EFF} values were obtained from ~~the~~ radiative transfer model simulations. The time series (1976−2023) of ~~these values and~~the conversion factors, RE_{EFF}~~(D)~~ ~~and~~(YR, MM, DD), and the corresponding noon value of the biologically effective irradiance, Ir_{EFF}~~$(t = \text{noon})$~~ ~~from Eq. (3–4)~~$(t = \text{noon}\,)$, have been archived in the IG PAS Data Portal (Krzyścin, 2024).

2.3.4 Regression models

~~Various~~The CCs described in section 2.3.2 were obtained for cloudless conditions and applied to all-sky conditions, where the contribution of the diffuse part of the radiation increases with cloud cover and dominates under overcast conditions. It cannot be excluded that the instruments used to monitor UVR at Belsk have their own specific characteristics for recording diffuse radiation, and that CF^*_{EFF} and CF_{EFF} in Eqs. (3−4) should also depend on the combined characteristics of clouds and instruments. To test whether this is the case, we investigated how different regression models ~~built from~~, which were trained using the ~~UV~~UVR data collected ~~in the~~between 2014 and 2023 (for this period ~~2014−2023 allowed for extended~~, the quality of the broadband radiometer was confirmed by the Brewer Mark II observations), reproduce the daily doses of erythemal ~~RE analysis for~~radiation throughout the ~~entire~~ 1976-2023 monitoring period ~~to provide a quality measure of the reevaluated UV~~.

The first model (Mod1) is based on clear-sky spectra determined with the RT model discussed in Section 2.3.1 and a cloud modification factor (CMF) derived from DCI data. The second and third models (Mod2 and Mod3) are based on TCO_3 and DCI data evaluated on a monthly basis. TCO_3 and DCI were either taken from observations at Belsk (Mod2) or ERA5 reanalysis (Mod3).

According to a ~~frequently~~widely used ~~UV~~UVR modelling concept (e.g. Rieder et al., 2008; den Outer et al., 2010; Čížková et al., 2018; Czerwińska and Krzyścin, 2024b) ~~that~~ the erythemal DRE on the current day ~~D~~, {YR, MM, DD}, RE_{ERYT}(~~D~~YR, MM, DD), is the product of ~~the so-called cloud modification factor (CMF), which is an~~ CMF (empirical function of ~~CI~~DCI parameterising UVR attenuation by clouds) for that day, and the synthetic clear-sky value~~,~~ $RE_{ERYT,CS}$~~(D)~~ (Section. 2.3.1):

$$RE_{ERYT}\text{~~}(D) = CMF\big(CI(D)\big)\text{~~}(YR, MM, DD) = CMF\big(DCI(YR, MM, DD)\big) \times RE_{ERYT,CS}\text{~~}(D),\text{~~}(YR, MM, DD), \quad (5)$$

$CMF(CI(D))$ is parameterisedcalculated here as a power function with the regression coefficients, α and β, depending on SZA at noon, SZA_N, for the current day D:{YR, MM, DD}:

$$CMF(CI(D))(DCI(YY,MM,DD)) = \alpha[CI(D)]^{\beta}\alpha[DCI(YY,MM,DD)]^{\beta}, \quad (6)$$

where estimates for the regression coefficients, α and β, were obtained from the 2014−2023 data when the KZ616 measurements were well=fitted matched to the BS64 data (Section 3.1). In CI calculations ($CI=GG_0DCI$ ($DCI=DG\,DG_0^{-1}$),) calculation, the daily integral of global solar DRE, G, comesirradiance, DG, is from observations at Belsk or ERA5, and its clear-sky equivalent, G_0DG_0, from ERA5 (before 1980), and thereafter the mean of ERA5 and MERRA-2 values.

The standard least-squares subroutine (Matlab function – *fitlm*(*x*,*y*)) provided the estimates for three arbitrarily selected SZA ranges (Table 12). These regression coefficients were used for the reconstruction of the $RE_{ERYT}(D)$ time series for the entire period of UVUVR measurements (1 January 1976 up to 31 December 2023). This model will be referred to as Mod1 in the following text.

Table 12. Estimates of the regression coefficients, α and β, describing the attenuation by the cloud of erythemal DRE by the empirical model, Mod 1, defined by Eqs. (5−6), for the three SZA ranges ofat noon SZA according to Eq. (6(SZAn).

Regression Coefficients					
α	β	α	β	α	β
SZA_N <45°		SZA_N≥45° and <60°		SZA_N≥60°	
0.954	0.844	0.918	0.750	0.960	0.697

The next two regression models were builttrained using the monthly averages of erythemal DRE, $RE_{ERYT}(YR,M)(YR,MM)$, for month MMM in year YR (from 2014 up to 2023) averaging all available daily $RE_{ERYT}(D)(YR,MM,DD)$ values in MMM month for YR year. The corresponding long-term (2014-2023) monthly means for M month, $RE^*_{ERYT}(M)(MM)$, is from the averages of all data for this calendar month. The idea of these models is to explain relative changes in the erythemal monthly RE, i.e., $\Delta ER(YR,MMM) = 100\%\,(RE_{ERYT}(YR,M)(YR,MM) - RE^*_{ERYT}(M)(MM))/RE^*_{ERYT}(M)(MM)$ with the corresponding relative changes in the UV explaining variables X, i.e., that affect UVR, $\Delta X(YR,M) = (YR,MM) = 100\%(X(YR,M)(YR,MM) - X^*(M)(MM))/X^*(M)(MM)$, where X={G, $X(YR,MM)$ is the monthly mean of DG or TCO_3}; in year YR and month MM and $X^*(MM)$ is the long-term monthly means for month MM

$$\Delta ER_K(YR,M)(YR,MM) = a_K(M)\,\Delta G(YR,M)(M)\,\Delta DG(YR,MM) + b_K(M)(MM)\Delta TCO_3(YR,M)(YR,MM) + c_k, \quad (7)$$

where K=OBS (for Mod2) and ERA5 (Mod3) are for the regression using the explaining variables from the measurements at Belsk and ERA5 reanalysis, respectively. Finally, the modelled $RE_{ERYT,K}$ (YR,M) value is equal to:

$$RE_{ERYT,K}(YR,M) = RE^*_{ERYT,K}(M)\left(1 + \frac{a_K(M)\,\Delta G(YR,M) + b_K(M)\Delta TCO_3(YR,M) + c_K}{100}\right), \quad (8)$$

$$RE_{ERYT,K}(YR,MM) = RE^*_{ERYT,K}(MM)\left(1 + \frac{a_K(MM)\,\Delta DG(YR,MM) + b_K(M)\Delta TCO_3(YR,MM) + c_K}{100}\right), \quad (8)$$

Models defined by Eq. (8) were used to compare fluctuations in UVUVR data in periods with RB and SL501 A measurements relative to the long-term monthly means in these periods, $RE^*_{ERYT}(M)RE^*_{ERYT,K}(MM)$, that were

approximated using the long-term averages of the measured RE_{ERYT}~~(D)~~(YR, MM, DD) values for the period 1976−1992 and 1993−2013, respectively. The regression coefficients, a_K, b_K, and c_K, which were calculated using the standard least-squares linear fit to the most reliable (2014−2023) data (Table ~~2~~3), were applied to construct monthly time series for the entire measurement period (1976−2023). ~~The model for K=OBS and ERA5 in Eq. (8) is denoted further in the text as Mod2 and Mod3, respectively.~~

Table ~~2~~3. Coefficients of the multilinear regressions derived for each calendar month based on the explaining variables from the measurements at Belsk (Mod2) and ERA5 reanalysis (Mod3) data for the period 2014−2023.

Month:	Mod 2			Mod 3		
	a_{OBS}	b_{OBS}	c_{OBS}	a_{ERA5}	b_{ERA5}	c_{ERA5}
January	0.84	−0.77	−5.69	1.34	−1.22	−8.38
February	0.81	−1.12	−0.12	0.95	−1.40	−0.05
March	0.59	−0.93	−0.65	0.84	−0.98	−0.77
April	0.90	−0.85	−1.94	1.26	−1.22	−3.77
May	0.86	−2.00	1.14	0.86	−1.97	0.64
June	1.08	−0.87	−0.05	1.14	−0.83	0.11
July	0.69	−0.84	0.00	0.40	−0.99	−0.00
August	0.82	−1.46	−1.99	0.63	−2.05	−1.40
September	0.86	−0.79	−0.00	0.94	−0.97	−0.00
October	0.80	−1.12	−0.49	0.86	−0.45	−0.52
November	0.58	−1.15	−1.02	0.66	−0.73	−0.97
December	0.73	−0.23	2.11	1.28	2.61	0.77

2.4 Statistical methods

Several standard statistical characteristics, which are calculated from the relative differences, z_i, between the observed, x_i, and model value, y_i, values expressed in percentage of the observed value, are used to determine the level of agreement between two time series. These are as follows: mean relative ~~error (MRE~~deviation (MRD), mean absolute ~~error (MAE~~deviation (MAD), standard ~~error (SE~~deviation (SD), root mean square ~~error (RMSE~~deviation (RMSD), and Pearson's correlation coefficient (R):

$$z_i = 100\%\frac{\sout{x_i - y_i}}{\sout{x_i}}\frac{y_i - x_i}{x_i}, \quad i = 1, \ldots, N., \tag{9}$$

$$\sout{MRE}MRD = \frac{1}{N}\sum_{i=1}^{N} z_i, \tag{10}$$

$$\sout{MAE}MAD = \frac{1}{N}\sum_{i=1}^{N} |z_i|, \tag{11}$$

$$SD = \sout{\left(\frac{1}{N}\sum_{i=1}^{N}(z_i - MRE)^2\right)^{\frac{1}{2}}}\left(\frac{1}{N}\sum_{i=1}^{N}(z_i - MRD)^2\right)^{\frac{1}{2}}, \tag{12}$$

$$\sout{RMSE}RMSD = \left(\frac{1}{N}\sum_{i=1}^{N} z_i{}^2\right)^{\frac{1}{2}}, \tag{13}$$

$$\sout{R = \frac{\sum_{i=1}^{N}(x_i - <x>)(y_i - <y>)}{\left(\sum_{i=1}^{N}(x_i - <x>)^2\right)^{\frac{1}{2}}\left(\sum_{i=1}^{N}(y_i - <y>)^2\right)^{\frac{1}{2}}}} R = \frac{\sum_{i=1}^{N}(y_i - <y>)(x_i - <x>)}{\left(\sum_{i=1}^{N}(y_i - <y>)^2\right)^{\frac{1}{2}}\left(\sum_{i=1}^{N}(x_i - <x>)^2\right)^{\frac{1}{2}}}, \; <x> = \frac{1}{N}\sum_{i=1}^{N} x_i, \; <y> = \frac{1}{N}\sum_{i=1}^{N} y_i, \tag{14}$$

Standard least-squares linear regression is applied to find the long-term tendency in the data. According to Weatherhead et al. (1998), the standard error of the linear trend estimate, SE_{LS}, by standard least-squares approach should be multiplied by the factor $F = \sqrt{(1+R_{k+1})/(1-R_{k+1})}$ to obtain the standard error corrected for the autocorrelation (with a time lag of 1) in the trend residuals, $SE_{LS,\,COR}$, if the trend residuals are positively correlated with the autocorrelation coefficient equal to R_{k+1}. F is set to 1 if the autocorrelation coefficient in the residual time series is negative.

$$SE_{LS,\,COR} = F \times SE_{LS}, \qquad (15)$$

Further in the text (Section 3.3), the slopes of the regression line will be calculated by Matlab function – *fitlm(x,y)*, and the corrected standard error of the slope, $SE_{LS,\,COR}$ for cases with $R_{k+1} > 0$, will be enlarged by the factor proposed by Weatherhead et al. (1998) (see Eq. (15)).

3 Results

3.1 The re-evaluation of the UVR measurements since 5 August 2013

On 5 August 2013, the KZ616 replaced the raw SL501 A #2011, which had been routinely used for UVR monitoring since 1995, as its performance had deteriorated (Fig. 2). Following this change, a new correction procedure for the Belsk's UVR meter was introduced for early detection of instrument failure. Each month its output (erythemal irradiance) was compared with the corresponding output of the collocated BS64. An example of such a monthly comparison (for June 2023) is shown in the scatter plot between the BS064 and KZ616 erythemal irradiances measured under clear-sky conditions (Fig.3a). In addition, Fig. 3b shows the monthly ratios between these clear sky erythemal irradiances for the entire BS and KZ comparison period (2014-2023).

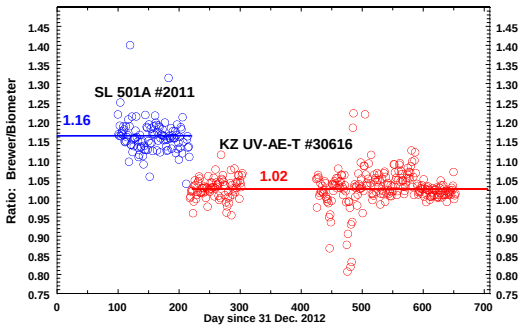

Figure 2. The ratio between the erythemal DRE from the ~~biometers~~erythemal radiometers (SL501 A #2011 before 5 August 2013 and KZ616 afterwards) and the Brewer Mark II spectrophotometer for the 2013−2014 period. The horizontal lines denote the mean value of the ratio.

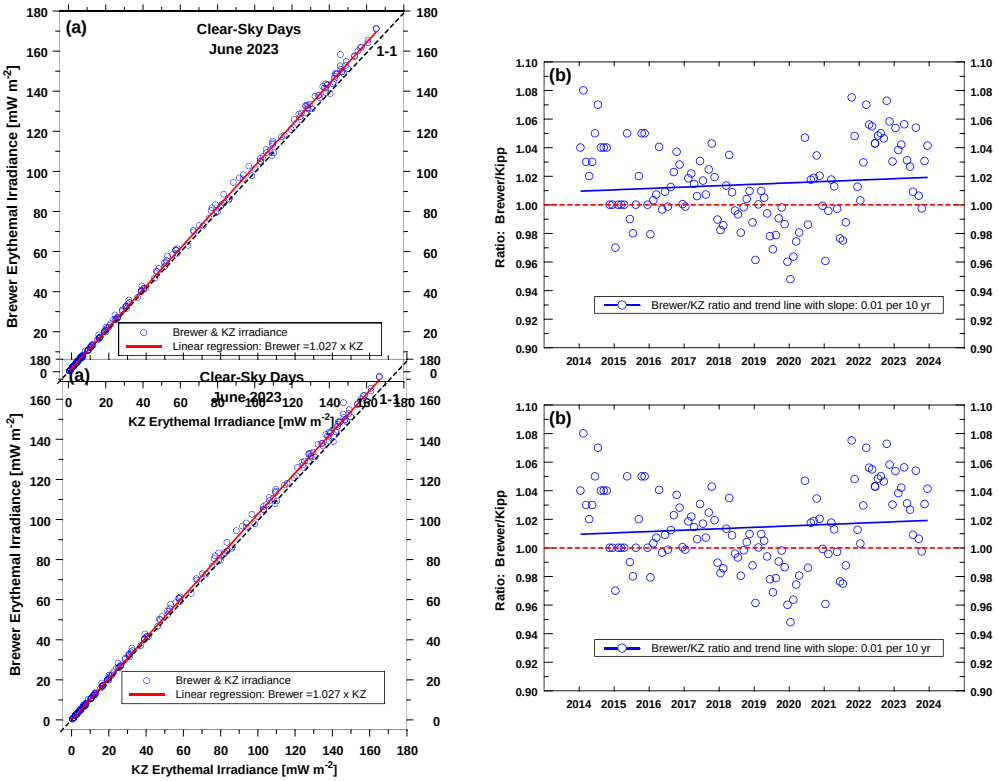

Figure 3. Comparison of the BS64 and KZ616 erythemal data for the period 2014−2023: (a) the ~~ratio between the~~ erythemal irradiances measured by the BS64 versus corresponding output of KZ 616 in June 2023 for clear-sky days,

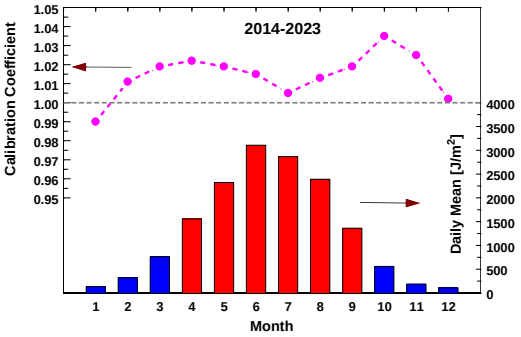

(b) time series of the monthly BS64/KZ616 ratios ~~for the 2014−2023 period.~~. The dashed line in Fig.3a shows the ideal 1:1 line.

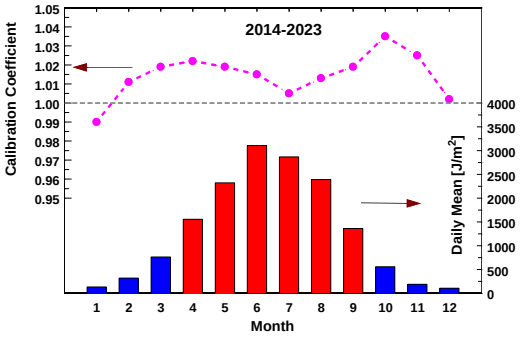

Figure 4. Seasonal pattern of the ~~calibration~~correction coefficient (~~CC ver. 1~~CC1) and daily erythemal RE for the period 2014–2023. Red bars denote months contributing mostly to the annual RE.

The long-term (2014–2023) means of the monthly CC1 and erythemal DRE for each calendar month are shown in the upper and lower graphs of Fig. 4. The ~~*CF*~~CC1 values are in the range of 1.00 to 1.02 during the period (April–September) when the intensity of solar ~~UV radiation~~UVR is usually high and the fine weather often allows

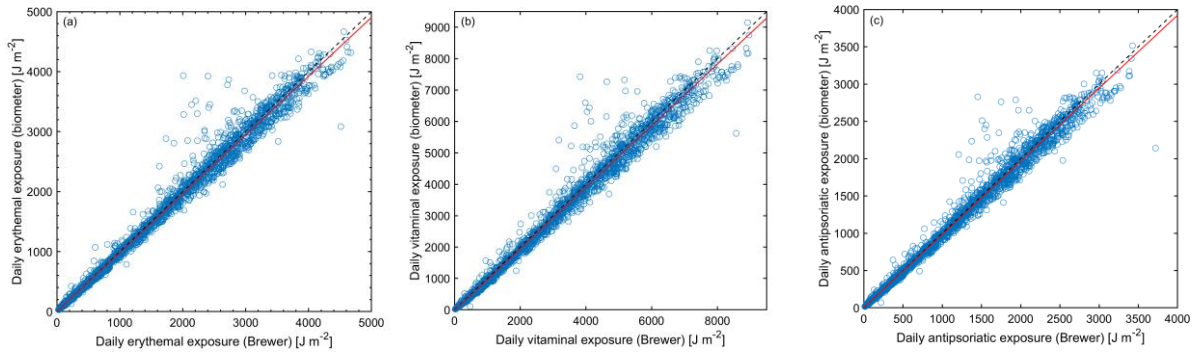

prolonged outdoor activity. Given this and the insignificant trend in the time series of the monthly BS64/KZ ratios (Fig. 3b), it was decided to keep the original KZ616 data without additional adjustments. This assumption is also supported by the BS64/KZ616 comparisons ~~for all BE data considered for the period 2014–2023,~~ as shown ~~by the linear regressions close to the 1:1 perfect agreement line~~ in the ~~three~~ scatter plots ~~(~~of Fig.-5~~).~~, which indicate that the Brewer and EBR data cluster about the ideal 1:1 line. For the daily vitamin D_3 and antipsoriatic RE, the values were reconstructed from the daily erythemal RE using the transfer coefficients defined by Eq. (4) (the values are archived in the IG PAS Data Portal, Krzyścin (2024), but the corresponding Brewer values were calculated from the real measured spectra weighted with the action spectra shown in Fig.1~~).~~.

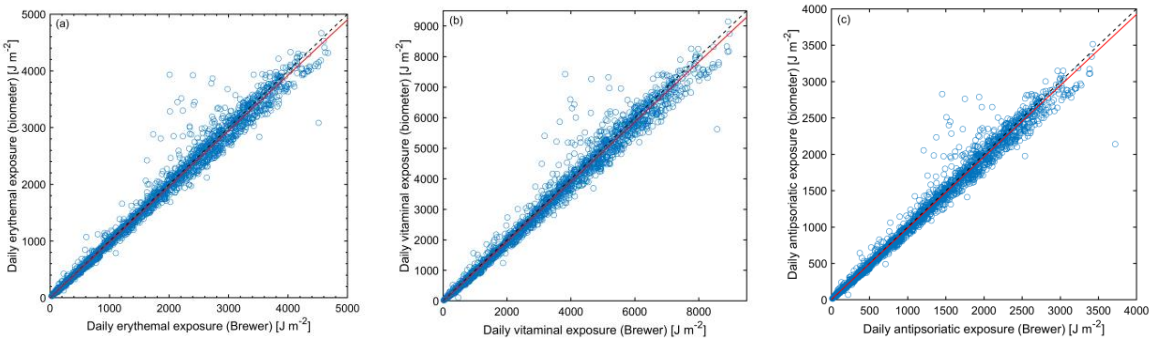

Figure 5. Scatter plots (KZ616 versus BS64) for biologically effective DRE in the period 2014–2023: (a) erythema ~~appearance~~, (b) previtamin D_3 synthesis, and (c) psoriasis clearance.

Table A1 shows the values of the descriptive statistics for the period 2014–2023 according to the different ranges of SZA values at noon (SZA_N), which confirm the good agreement between the DRE for all considered biological effects from the well-calibrated BS64 and KZ616 measurements used in routine ~~UV~~UVR monitoring. For example, regardless of the biological effect, ~~MRE~~MRD and ~~RMSE~~RMSD are ~ −1 % and ~9 % for SZA_N <45°, which occurs from 8 April to 5 September at Belsk, i.e. during the period with the highest ~~UV~~UVR intensity of the year. For $SZA_N \geq 60°$ (from 15 October up to 27 February of next year), ~~MRE~~MRD and ~~RMSE~~RMSD are only slightly larger (~ −2 % and ~10 %, respectively) for the erythema and antipsoriatic exposures. These values are higher (~ −13 % and ~18 %) for the previtamin D_3 exposures, raising questions about the usefulness of the

erythema ~~biometers~~radiometers for measuring vitamin D_3 exposure~~.~~ when $SZA_N \geq 60°$. However, vitamin D_3 synthesis in the skin ceases during this period.

3.2 The ~~recevaluation~~re-evaluation of the ~~UV~~UVR measurements before 5 August 2013

3.2.1 ~~Calibration~~Correction coefficients from the clear-sky model simulations

Analyses of intraday ~~UV~~UVR measurements in Belsk from 1 January 1976 to 4 August 2013 have to be divided into two parts, i.e. 1 January 1976–31 December 1992, and 1 January 1993–4 August 2013, due to the different broadband instruments used for ~~UV~~UVR monitoring. In the first period, daily erythemal exposures were archived on the basis of manual summation of RB counts per day. For the latter period, 1-min erythemal irradiances were automatically recorded by a logger using SL501 A biometers and utilized in the calculation of ~~UVI~~UVI_{MAX} and daily erythemal RE. Two methods of data ~~calibration for the period 1976–2013 are~~correction were proposed (Sect. 2.3.2) using clear-sky data: modelled and measured daily erythemal RE ~~and UVI~~(for the period 1976-2013) and UVI_{MAX} (1993-2013) for the correction method denoted CC1 and CC2, respectively. Figure 6a shows the time series of CC1 and CC2 values together with their smoothed values by the ~~LOcally Weighted Scatterplot Smoothing~~ ~~(~~LOWESS~~)~~ smoother, ~~Cleveland (1979),~~ which were used as multipliers of the raw ~~UV~~UVR data before 5 August 2013. The ~~differences~~difference between CC1 and CC2 are shown in Fig. 6b.

In the ~~former~~1976-1992 period, UVI values were not archived. This means that CC2 values cannot be directly calculated. However, CC2 values equal to 1 could be assumed as the output of the RB instrument was previously adjusted to that by SL501 A #927 using their simultaneous measurements for the period 1992−1994 (Puchalski et al., 1995). Such an assumption can also be supported here by a small jump (~1-%) in the ~~differences~~difference between the CC1 and CC2 values in January 1993 (Fig. 6b). This jump is really small taking into account that the 1993 adjustment of RB meter was inferred from field comparisons between RB and SL501 A #927 but here this

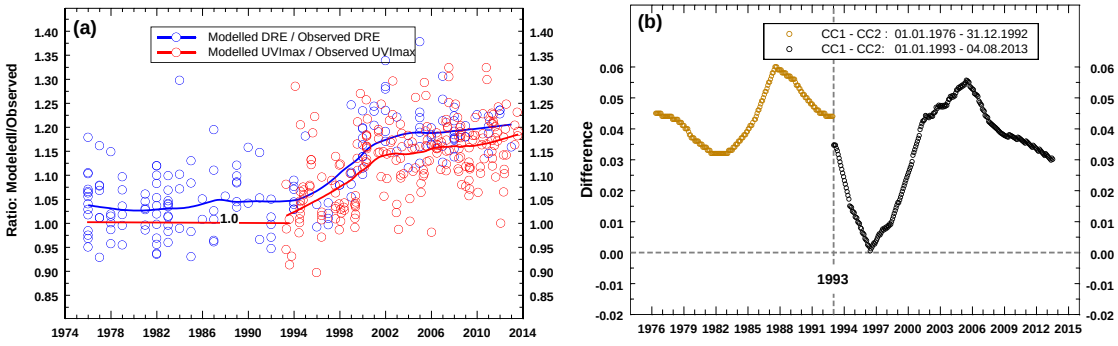

is calculated from smoothing ratios between modelled and observed UVI at noon for clear-sky days. Moreover, in the period 1976−~~1993~~1992, an oscillation with 0.015 amplitude is seen around the constant level of CC1=1.045 which justifies the assumption of an almost constant CC2 pattern before 1993. Using two sets of the ~~recevaluated~~re-evaluated 1976−2013 data will allow us to discuss the robustness of trend calculations for the entire 1976−2023 period of the ~~UV~~ UVR measurements at Belsk (Sect. 3.3).

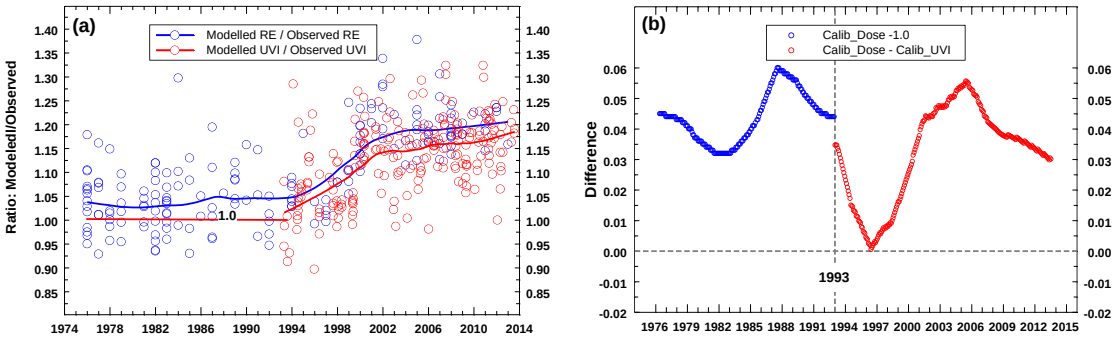

Figure 6. (a) TUV model-observation ratios for erythemal DRE and noon UVI obtained for clear-sky days. The solid curves represent smoothed values of the ratios to be used as the ~~calibration~~correction coefficients, i.e., the multipliers applied to the raw measurements. The multipliers were set equal to 1 for the 1976−~~1993 calibration~~1992 correction based on ~~UVI~~ratios of noon UVIs, (b) ~~differences~~difference between the monthly means of the ~~calibration~~correction coefficients shown in Fig.6a.

3.2.2 ~~Statistical~~Performance of the regression models

Erythemal DRE for the period 1 January 1976 – 4 August 2013 were reconstructed with Mod1 defined by ~~Eq.(~~Eqs. (5~~)−(~~−6). The model's constants came from the model training using the original KZ data and the explaining variables (TCO_3 and ~~CI~~DCI) from 5 August 2013 − 31 December 2023 period. The reconstructed values were compared with two sets of the ~~reevaluated~~re-evaluated data obtained before 5 August 2013 after multiplying raw daily erythemal RE with CC1 and CC2, respectively.

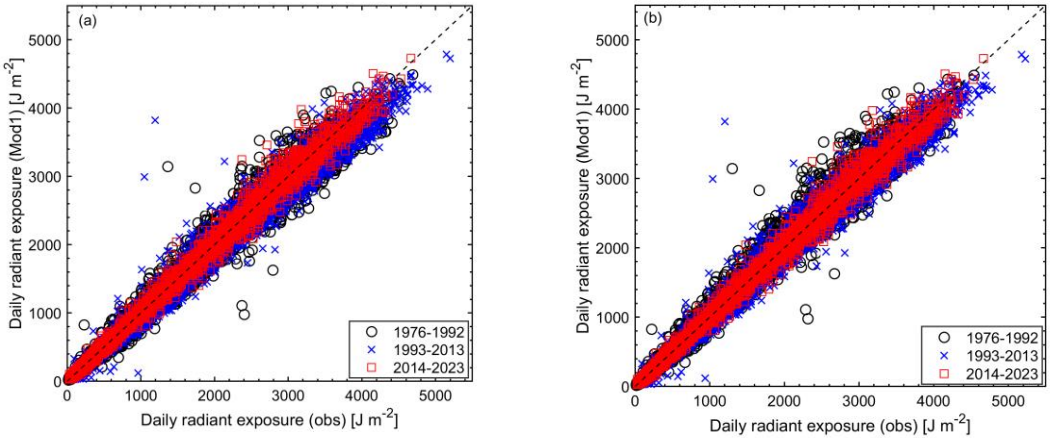

~~Figure 7. Scatter plot of the modelled (Mod1) erythemal DRE versus the re-evaluated observed values for the 1976−1992, 1993−2013, and 2014−2023 period, respectively: (a) CC1 version of the correction coefficients for the period 1 January 1976−4 August 2013, (b) corresponding CC2 version of the correction coefficients. KZ616 measurements were taken without corrections.~~

Figure 7 shows the scatter plot of the reconstructed (Mod1) versus ~~reevaluated~~re-evaluated erythemal DRE with CC1 (Fig.7a) and CC2 (Fig.7b) multipliers of the raw data for the three periods corresponding to the RB, SL501A, and KZ616 measurements, respectively. The points in Figure 7 cluster around a line of perfect 1-1 agreement with only a few outliers. It seems that there is only a small difference between the ~~reevaluated~~re-evaluated daily erythemal RE and the corresponding output of Mod1 with the CC1 and CC2 multipliers. This is also supported by similar values of the descriptive statistics for the periods 1976−1992 and 1993−2013 (Table ~~3~~4). It is worth mentioning that the performance of Mod1 ~~resembles~~in the period 2014−2023 is similar to that of the Brewer

spectrophotometer ~~from the comparison~~that was found when compared with the original KZ616 data (~~see almost~~note the ~~same~~close values of the descriptive statistics for the ~~full~~ year-round data in column "CC=1" of Table ~~3~~4 and Table A1 for the ~~"~~"All ~~SZA_N~~"SZA_N" cell~~,~~ and column "Eryt", for example, ~~RMSE~~RMSD values are equal to 10.5 % and 8.9 %, respectively).

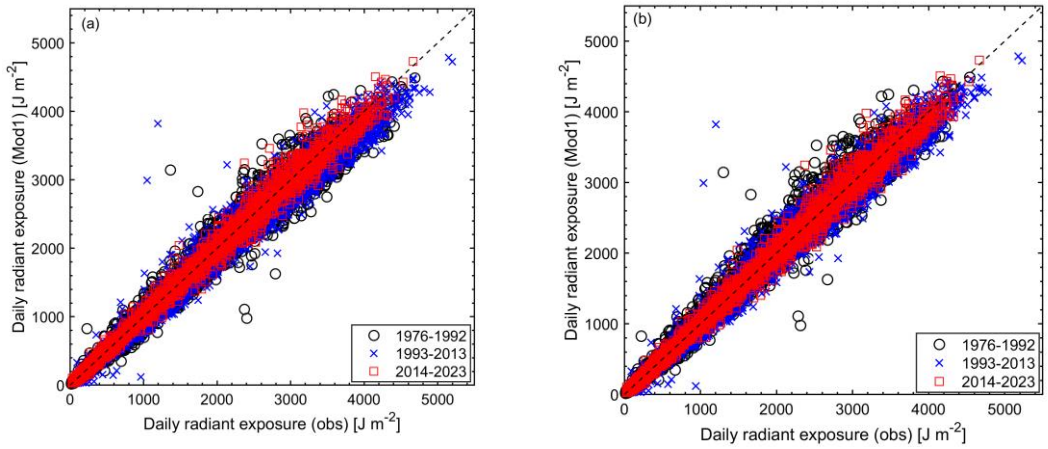

~~**Figure 7. Scatter plot of the modelled (Mod1) erythemal DRE versus the reevaluated observed values for the 1976–1992, 1993–2013, and 2014–2023 period, respectively: (a) CC1 version of the calibration coefficients for the period 1 January 1976–4 August 2013, (b) corresponding CC2 version of the calibration coefficients. KZ616 measurements were taken without corrections.**~~

Table ~~3~~4. The descriptive statistics (~~MRE, MAE, RMSE~~MRD, MAD, RMSD~~, as defined in Sect. 2.4~~) calculated from the relative daily differences, 100% (~~reevaluated~~Mod1 value – re-evaluated measurement~~ – Mod1 value)/(reevaluated~~)/(re-evaluated measurement), for the periods 1976–1992, 1993–2013 and 2014–2023. The correlation coefficient R was obtained from the ~~reevaluated~~re-evaluated measurements and modelled values. Two versions of the ~~reevaluated~~re-evaluated datasets were considered, using CC1 and CC2 multipliers on the raw measurements. Both datasets include raw KZ616 data as there was no need to recalculate these data. The results are shown for annual (January–December) and summer (June–August) data.

Statistics	Year-Round (January–…–December)					June–July–August				
	Multipliers of the raw data									
	1976–1992		1993–2013		2014–2023	1976–1992		1993–2013		2014–2023
	CC1	CC2	CC1	CC2	CC=1	CC1	CC2	CC1	CC2	CC=1
~~MRE~~MRD	–2.7	–1.6	–1.9	–0.3	–1.4	–0.8	–3.5	–2.6	–1.0	–0.9
~~MAE~~MAD	9.8	9.6	9.7	9.4	6.8 10.5	7.8	8.1	7.0	6.4	5.2
~~RMSE~~RMSD	13.7	14.1	14.5	14.6	1.00 10.4	10.8	11.7	10.1	9.7	6.9
R	1.00	0.99	1.00	0.99		0.96	0.96	0.97	0.98	0.98
SD	13.4	14.0	14.3	14.6		10.9	11.2	9.8	9.7	6.8

Erythemal DRE by Mod1 can be obtained for days when the explanatory variables, TCO_3 and ~~CI~~DCI, are available from the collocated measurements at Belsk by the Dobson radiometer and pyranometer, respectively. It is therefore possible to fill gaps in the measured data and obtain a complete (1976–2023) series of erythemal DRE to be used in calculations of erythemal annual and summer (June–July–August) RE. These ~~data~~REs can also be calculated using the erythemal monthly RE based on Mod2 and Mod3. All these series are analysed in ~~section~~Section 3.3 for trend calculations to assess the level of uncertainty in the long-term variability of the Belsk ~~UV~~UVR data.

Table ~~4~~5 shows the values of the descriptive statistics for the three models used (Mod1, Mod2 and Mod3) and two versions of the ~~reevaluated~~re-evaluated data (using CC1 and CC2 multipliers on the raw data) based on the annual and summer RE. The differences between descriptive statistics (~~MRE, MAE, RMSE~~MRD, MAD, RMSD, SD) in CC1 and CC2 columns are within a few percentage points for ~~MRE~~MRD and about 1−1.5 percentage points for other statistics, indicating that the ~~two independent calibration~~different correction methods give fairly similar results. The performance of Mod2 and Mod3 is in most cases slightly better than that of Mod1 (Table ~~4~~5) because these models add fluctuations to the mean values for the periods 1976–1992, 1993–2013 and 2014–2023 calculated from the ~~reevaluated~~re-evaluated measurements of RB, SL501A (#919 and #2011 for the periods 1993–1994 and 1995–2013 respectively) and the original KZ616 measurements.

All models considered were designed to test whether changes in the primary ~~UV~~UVR drivers, ozone and clouds, explain year-to-year ~~UV~~UVR variability. The performance of Mod3 is surprisingly similar to that obtained from Mod2 despite the use of ~~UV~~UVR proxies (TCO_3 and DGI) from the ERA5 reanalysis~~. This confirms the possibility of using explanatory variables from these reanalyses to fill gaps in the proxy data~~.

The lowest correlation coefficients between the ~~reevaluated~~re-evaluated measurements and modelled values were found in the period 1993−2013 for the measurement-model pairs with the same version of the CC multipliers (CC1 or CC2). This is particularly pronounced for the summer data (see e.g. Mod3 values of 0.50 and 0.43 for CC1 and CC2 pairs, respectively), suggesting a poorer agreement between measurements and model in the period 1993−2013. This was found for all models. However, other descriptive statistics (~~MRE, MAE, RMSE~~MRD, MAD, RMSD and SD) differed only slightly, i.e. less than 1.5 percentage points~~.~~, when values in CC1 and CC2 columns were compared.

Table ~~4~~5. Same as Table ~~3~~4, but the descriptive statistics are calculated using time series of erythemal annual and summer RE.

Statistics	Year-Round: January−…−December					Summer: June−July−August				
	Multipliers of the raw data									
	1976−1992		1993−2013		2014−2023	1976−1992		1993−2013		2014−2023
	CC1	CC2	CC1	CC2	CC=1	CC1	CC2	CC1	CC2	CC=1
					Mod1					
~~MRE~~MRD	−3.3	=0.9	−4.2	−2.6	−0.2	−1.9	=2.4	−3.5	−1.9	=0.5
~~MAE~~MAD	3.9	2.5	4.7	3.2	1.0	4.0	3.4	4.4	2.8	1.8
~~RMSE~~RMSD	4.4	2.9	5.0	3.5	1.2	4.4	4.5	4.8	3.4	2.6
R	0.82	0.86	0.77	0.83	0.93	0.92	0.93	0.57	0.65	0.96
SD	3.2	3.0	2.8	2.4	1.4	4.2	4.0	3.3	2.9	2.7
					Mod2					
~~MRE~~MRD	−0.9	−1.0	−0.5	−0.6	−0.3	−1.0	−1.1	−0.6	−0.6	=0.0
~~MAE~~MAD	2.1	2.0	2.0	1.8	0.6	3.3	2.9	2.2	1.9	1.3
~~RMSE~~RMSD	2.6	2.4	2.7	2.3	0.8	4.0	3.7	2.8	2.4	1.8
R	0.90	0.92	0.81	0.86	0.97	0.93	0.94	0.72	0.79	0.98
SD	2.6	2.4	2.7	2.3	0.8	4.1	3.7	2.8	2.4	1.9
					Mod3					
~~MRE~~MRD	−0.4	−0.5	−0.9	−0.9	−0.6	=0.2	=0.1	−0.3	−0.3	=0.1

~~MAE~~MAD	1.5	1.4	2.7	2.8	0.8	3.0	3.2	2.9	2.9	2.1
~~RMSE~~RMSD	1.7	1.9	3.4	3.6	0.9	3.7	3.7	3.7	3.7	2.5
R	0.96	0.94	0.70	0.67	0.97	0.94	0.94	0.50	0.43	0.92
SD	1.8	2.0	3.4	3.5	0.8	3.9	3.9	3.8	3.8	2.7

3.3 Trend analyses

3.3.1 The erythemal annual and summer radiant exposures in the period 1976-2023

Trend analyses are applied to the erythemal annual and summer RE based on daily ~~(for reevaluated~~RE. There are two series to be considered when dealing with the measured data. The first, labelled OBS, uses only re-evaluated observations ~~with filled gaps, $OBS_{F,}$~~ and ~~Mod1) and~~the monthly ~~RE (for Mod2 and Mod3). Gaps in the measurements were filled using Mod1~~average is calculated when at least 14 daily ERE values are available. The second one, $OBS_{F,}$ contains all the daily gaps filled by Mod 1 simulations. ~~Two versions of the $OBS_{F,}$ Mod2 and Mod3 time series are possible because of the use of CC1 and CC2 multipliers on~~ For other models used there are no gaps. In case of Mod1, erythemal annual and summer RE are built using the ~~raw (1976−2013)~~re-evaluated daily ~~measurements~~ERE values. For Mod2 and Mod3, the ~~Mod1 time series, only one series was available for analysis, as this model~~monthly reconstructed ~~erythemal~~ RE ~~using~~values are summed over the ~~proxy values and the model coefficients estimated from the KZ616 measurements (2014−2023), which did not require calibration.~~ year and summer season.

~~For Mod2 and Mod3, two variants of the time series were available as these models required the 1976−1992 and 1993−2013 mean values taken from the reevaluated measurements with two possible options (CC1 or CC2) for the calibration multipliers.~~ The 1976−2023 time series for the erythemal annual and summer RE using CC1 and CC2 ~~calibration~~correction multipliers are shown in Fig. 8 and Fig. A1, respectively. Fig.8a (Fig.A1a) and Fig.8b (Fig.A1b) are for the erythemal annual (and summer) RE.

Linear regression lines are superimposed on the graphs to illustrate the long-term variability in the time series. Two independent lines are drawn to account for a change in the trend pattern observed in the time series somewhere in the early 2000s. The year of the trend change was calculated by examining the performance of fifteen combinations of this two-line pattern, varying the year of the trend change point (from 1995 to 2009). The best fit with maximum coefficients of determination ~~coefficients~~ was found for the trend change point in 2005. Therefore, the slopes of the regression lines (in kJ m^{-2} per year) and the trend values (in % per year) shown in Table ~~5~~6 and Table ~~6~~7, respectively, are calculated for the 1976−2004 and 2005−2023 periods. Standard ~~deviations~~errors of the trend estimates are calculated according to Eq. (15) ~~if the consecutive values~~ accounting for the correction for the autocorrelation in the trend residuals ~~are positively correlated, i.e.~~if the autocorrelation coefficient with 1-yr lag, R_{k+1} ~~> 0~~, is positive (also shown in Tables ~~4~~−5−6).

The interannual variations and trend lines of erythemal annual RE are close to each other when comparing the upper graphs in Fig. 8 and Fig.A1. This can also be observed for the summers when comparing the corresponding lower plots. At the beginning of the RB observations (1976−1986), there were large oscillations from year to year, suggesting an instrumental problem with the data. However, all modelled time series show quite similar oscillations for this period, supporting the ~~thesis~~hypothesis that a specific combination of TCO_3 and cloud transparency may be responsible for such oscillations.

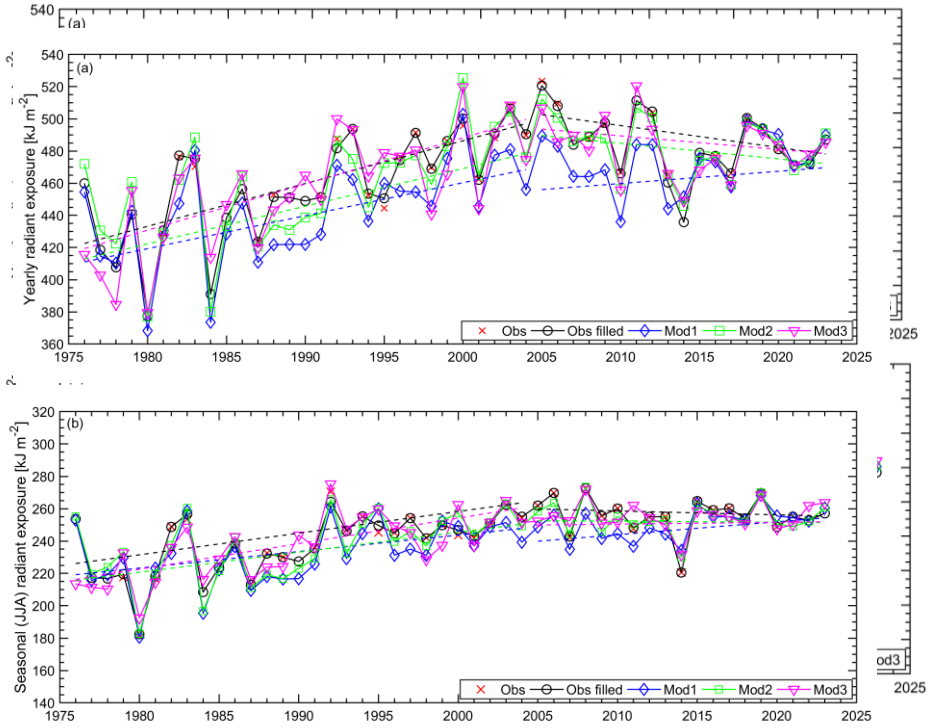

Figure 8. Time series (1976−2023) of the erythemal radiant exposures from ~~reevaluated~~re-evaluated observations (Obs), ~~reevaluated~~re-evaluated observations with filled gaps (Obs filled), and model estimates (Mod1, Mod2, and Mod3) using the CC1 version of the ~~calibration~~correction coefficients: (a) annual (January−December) radiant exposures; (b) summer (June−Aug) radiant exposures. Dashed lines represent the linear trends calculated for the period 1976−2004 and 2005−2023.

The slopes of the linear fit to the analysed time series (Table ~~5~~6) show a statistically significant positive trend between 1976 and 2004 of around 20−30 kJ m^{-2} and 10−20 kJ m^{-2} per decade in the annual and summer data, respectively. The trends are mostly insignificant for the period 2005−2023, with only one exception (for the Mod1 data) with a continued positive trend of ~ 10 kJ m^{-2} per decade. The corresponding trend values expressed in dimensionless units (Table ~~6~~7) have the same values of about 4−7% per 10 years in the former period for both the annual and summer time series. In the latter period, the positive trend of Mod1 is ~3 % per 10 years. ~~The smallest~~Mod 1 and Mod 3 (with CC2) gave the ~~largest~~lowest and highest trends ~~are always provided by Mod1 and Mod3 with CC2 calibration coefficients~~, respectively. However, the differences between these trends are within the range of ± 2 standard errors of the trend estimates, taking into account the autocorrelation in the residuals of the models (column $SE_{LS, COR}$ in Table ~~5~~6).

By averaging all available statistically significant annual and summer trend values shown in the third and seventh columns of Table ~~5~~6 and Table ~~6~~7, the following trends and their standard errors are obtained: for the period 1976–2004: 27.4 ± 4.4 kJ m^{-2} and 5.64 ± 0.92 % per decade for the erythemal annual RE, and 14.3 ± 4.3 kJ m^{-2} and 5.63 ± 1.03 % per decade for the erythemal summer RE. These values correspond to the average trend from the two series based only on the ~~reevaluated~~re-evaluated measurements (OBS_F values in the Tables), i.e. 28.7 kJ m^{-2} and 5.9 % per decade for the erythemal annual RE, and 14.3 kJ m^{-2} and 5.6 % per decade for the erythemal summer RE.

Table ~~5~~6. Trends (kJ m^{-2} per year) by the linear least-squares fit to the time series of erythemal annual and summer radiant exposures shown in Fig.8 and Fig.A1 calculated for the periods 1976–2004 and 2005–2023. $SE_{LS,\,COR}$ denotes the standard error of the trend estimate taking into account the autocorrelation (with a lag of 1 year) in the series of the residuals of the trend model. R_{k+1} denotes the correlation coefficient in the lagged residuals. Bold font indicates a statistically significant trend value at the 2-sigma level.

Data Type	Correct. Method	Annual (January...–...December) sum [kJ m^{-2}]				Summer (June–July–August) sum [kJ m^{-2}]			
		$Trends_{1976–2004}$		$Trends_{2005–2023}$		$Trends_{1976–2004}$		$Trends_{2005–2023}$	
		Trend ± $SE_{LS,\,COR}$	R_{k+1}	Trend ± $SE_{LS,COR}$	R_{k+1}	Trend ± $SE_{LS,\,COR}$	R_{k+1}	Trend ± $SE_{LS,\,COR}$	R_{k+1}
OBS_F	CC1	**2.66 ±0.52**	−0.11	−1.36 ±0.98	0.17	**1.34 ±0.37**	0.08	−0.24 ±0.49	−0.32
	CC2	**3.08 ±0.52**	−0.06	−0.45 ±0.87	0.14	**1.52 ±0.37**	0.07	−0.26 ±0.48	−0.30
Mod1	–	**2.05 ±0.57**	−0.19	0.76 ±0.78	0.08	**1.02 ±0.38**	−0.13	**0.80 ±0.36**	−0.20
Mod2	CC1	**2.34 ±0.61**	−0.16	−0.97 ±0.85	0.12	**1.24 ±0.39**	−0.08	−0.06 ±0.41	−0.38
	CC2	**2.84 ±0.61**	−0.10	−0.30 ±0.79	0.10	**1.50 ±0.39**	−0.01	0.29 ±0.41	−0.32
Mod3	CC1	**2.84 ±0.56**	−0.21	−0.84 ±0.76	−0.08	**1.58 ±0.32**	0.02	0.11 ±0.37	−0.13
	CC2	**3.34 ±0.54**	−0.22	−0.17 ±0.72	−0.13	**1.82 ±0.20**	0.05	0.46 ±0.36	−0.13

Table ~~6~~7. Same as Table ~~5~~6, but the results are for the trend values expressed in % per year.

Data Type	Correct. Method	Annual (January..–..December) sum [% yr^{-1}]				Summer (June–July–August) sum [% yr^{-1}]			
		$Trends_{1976–2004}$		$Trends_{2005–2023}$		$Trends_{1976–2004}$		$Trends_{2005–2023}$	
		Trend ± $SE_{LS,\,COR}$	R_{k+1}	Trend ± $SE_{LS,\,COR}$	R_{k+1}	Trend ± $SE_{LS,\,COR}$	R_{k+1}	Trend ± $SE_{LS,\,COR}$	R_{k+1}
OBS_F	CC1	**0.54 ±0.11**	−0.11	−0.28 ±0.17	0.17	**0.52 ±0.14**	0.08	−0.09 ±0.19	−0.32
	CC2	**0.64 ±0.11**	−0.06	−0.09 ±0.16	0.14	**0.60 ±0.14**	0.07	0.10 ±0.19	−0.30
Mod1	–	**0.42 ±0.12**	−0.19	0.16 ±0.15	0.08	**0.40 ±0.15**	−0.13	**0.31 ±0.14**	−0.20
Mod2	CC1	**0.48 ±0.13**	−0.16	−0.20 ±0.15	0.12	**0.49 ±0.15**	−0.08	−0.02 ±0.16	−0.38
	CC2	**0.59 ±0.12**	−0.10	−0.06 ±0.15	0.10	**0.59 ±0.15**	−0.01	0.11 ±0.16	−0.32
Mod3	CC1	**0.59 ±0.12**	−0.21	−0.17 ±0.16	−0.08	**0.62 ±0.12**	0.02	0.04 ±0.15	−0.13
	CC2	**0.69 ±0.11**	−0.22	−0.04 ±0.15	−0.13	**0.72 ±0.13**	0.05	0.18 ±0.14	−0.13

3.3.2 The vitamin D_3 and antipsoriatic annual and summer radiant exposures in the period 1976-2023

The ~~standard biometer~~commercial EBRs used to monitor erythemal irradiance can also measure non-erythemal irradiance (Czerwińska and Krzyścin, 2024a). Figure 5 and Table A1 provide that the daily vitamin D_3 and antipsoriatic RE derived from the KZ616 measurements agree with the directly measured BS64 values in the same way as the original (erythemal) KZ616 data. This supports the method of the transfer from erythemal irradiance to non-erythemal irradiance proposed by Czerwińska and Krzyścin (2024a).

Figure 9 shows the time series of ~~the~~ annual and summer values of ~~the~~ previtamin D_3 synthesis and psoriasis healing RE from 1976 to 2023. It ~~looks like~~appears that these time series are very similar ~~when comparing the~~

~~vitamin D3 to the antipsoriatic time series. Moreover~~. In addition, these time series are similar to the erythemal series shown in Fig.8. The correlation coefficients between the pairs of time series shown in Fig.8 and Fig.9, i.e. erythema & vitamin D_3, erythema & psoriasis, vitamin D_3 & psoriasis, ~~are~~were in the range [0.90, >0.999] with the ~~smallest~~lowest value for the ~~cases of~~ erythema & vitamin D_3~~,~~ and erythema & psoriasis ~~calculations using~~pairs when the summer data from Mod1 simulations were considered.

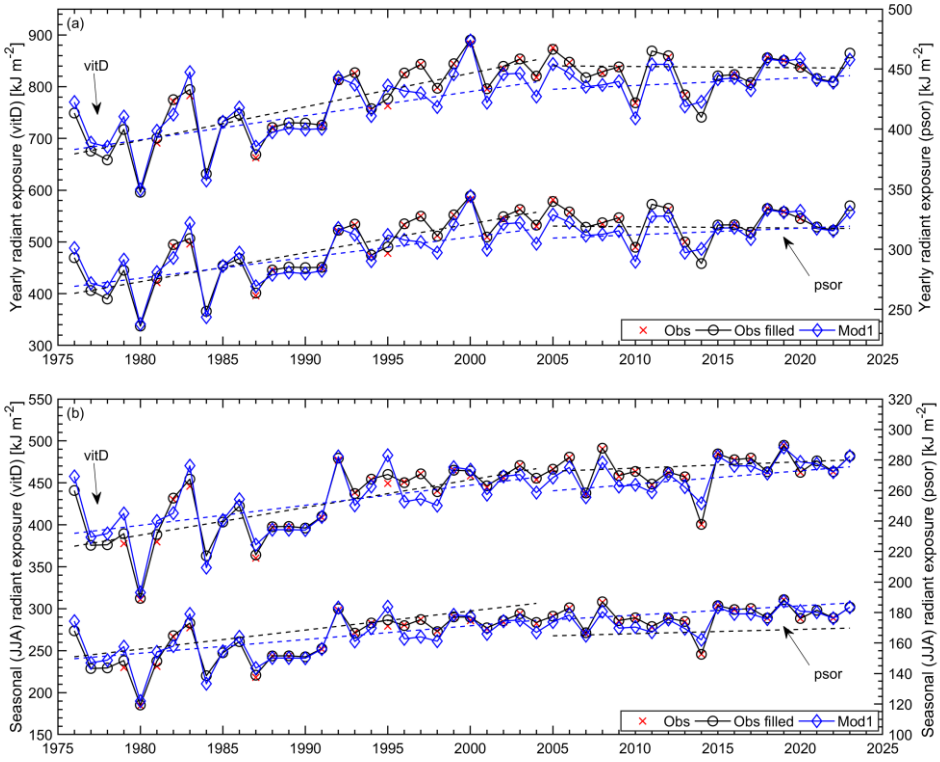

Figure 9. Time series (1976−2023) of the previtamin D_3 synthesis and psoriasis healing radiant exposures from ~~reevaluated~~re-evaluated observations (Obs), ~~reevaluated~~re-evaluated observations with filled gaps (Obs filled), and model Mod1 estimates (Mod1) using the CC2 version of the ~~calibration~~correction coefficients: (a) annual (January−December) radiant exposures; (b) summer (June-July-August) radiant exposures. Dashed lines represent the linear trends calculated for the period 1976−2004 and 2005−2023.

Table ~~7~~8 shows the trend values for the period 1976-2004 and 2005-2023 from the time series calculated using the erythemal DRE multiplied by the transfer coefficients defined by Eq. (4). The transfer coefficients depend on only two parameters (TCO_3 and SZA), even on cloudy days, as previously shown by Czerwińska and Krzyścin (2024a). The statistically significant trend values for previtamin D_3 synthesis and psoriasis clearance are slightly higher, by about 1−1.5 percentage points per decade, than the corresponding trend values for the erythema ~~appearance~~ shown in Table ~~6~~7. Taking into account the standard error of the trend estimate of about 1% per decade, it cannot be said that the differences between the trends are statistically significant.

Table ~~7~~8. Same as Table ~~6~~7, but trend values are for previtamin D_3 synthesis and psoriasis clearance.

Data Type	Correct. Method	Annual (January−December) RE [% per year]				Summer (June−July−August) RE [% per year]			
		$Trends_{1976-2004}$		$Trends_{2005-2023}$		$Trends_{1976-2004}$		$Trends_{2005-2023}$	
		Trend ± $SE_{LS, COR}$	R_{k+1}	Trend ± $SE_{LS, COR}$	R_{k+1}	Trend ± $SE_{LS, COR}$	R_{k+1}	Trend ± $SE_{LS, COR}$	R_{k+1}

				Previtamin D_3 synthesis					
OBS_F	CC1	**0.70 ±0.12**	−0.12	−0.27 ±0.22	0.12	**0.64 ±0.16**	0.06	−0.07 ±0.20	−0.25
	CC2	**0.77 ±0.12**	−0.07	−0.03 ±0.19	0.08	**0.71 ±0.15**	0.05	0.16 ±0.19	−0.32
Mod1	–	**0.56 ±0.14**	−0.20	0.17 ±0.16	0.02	**0.51 ±0.16**	−0.15	**0.34 ±0.14**	−0.18
				Psoriasis clearance					
OBS_F	CC1	**0.66 ±0.12**	−0.13	−0.27 ±0.21	0.15	**0.63 ±0.15**	0.06	−0.07 ±0.20	−0.25
	CC2	**0.74 ±0.12**	−0.08	−0.03 ±0.20	0.10	**0.70 ±0.15**	0.05	0.16 ±0.19	−0.26
Mod1	–	**0.53 ±0.13**	−0.20	0.17 ±0.18	0.14	**0.51 ±0.16**	−0.15	**0.34 ±0.14**	-0.18

4 Summary and Discussion

~~One of the world's longest measurements of solar UV radiation at the Earth's surface (and probably the longest taken by erythemal biometers) comes from Belsk.~~ ~~Measurements began in 1975 and continuous monitoring started on 1 January 1976.~~ ~~To the authors' knowledge, the longest UV monitoring series began in Moscow in 1968 with a broadband (300−380 nm) instrument developed at the Moscow State University Meteorological Observatory (Chubarova et al., 2000).~~

~~Several biometers participated in UV monitoring at Belsk, starting with RB, which operated until 31 December 1992. Subsequently, biometers SL501 A (#919 and #2011) and, since 5 August 2013, KZ616 have participated in UV monitoring. Each of these instruments has individual characteristics (spectral response, cosine error, ageing rate) and technical solutions, e.g. RB was not temperature stabilised and its output was in solar burn units. Therefore, a retrospective re-evaluation of the Belsk UV time series was necessary, and the homogenisation of the data from 1976 to 2023 is presented in this article.~~

Belsk is a unique observatory where ~~UV~~UVR monitoring has been accompanied by monitoring of ozone (TCO_3), aerosol optical properties (AOD) and cloud characteristics (sunshine duration, ~~CI~~DCI from global solar irradiance measurements), i.e. basic input parameters to a radiative transfer model allowing reconstruction of the erythemal RE. In addition, collocated BS64 measurements of ~~UV~~UVR spectra ~~allow monthly verification~~are used in the frequent (every month) checking of actual KZ616 performance. BS64 spectral measurements also allow assessment of the quality of Czerwińska and Krzyścin (2024a) retrieval to convert standard erythemal measurements to the non-erythemal BE irradiance (see the cases of the vitamin D_3 and antipsoriatic DRE in Figure 5).

~~Model simulations of erythemal DRE and UVI under cloudless sky provide a basis for the correction procedure of raw UV data. A selection of clear-sky conditions throughout the entire day from the daily proxy values (relative sunshine duration and RE from global solar irradiation), which were available for Belsk, is not straightforward as only the examination of the daily course of these measurements would allow to capture cloudless moments within the day. Therefore, two very different calibration configurations~~Two sets of raw UVR data multipliers (CC1 and CC2 as defined in section 2.3.2) have been proposed to assess the uncertainty range of the ~~calibration~~correction method~~.~~ applied to the raw UVR data. The ~~reevaluated~~re-evaluated time series appear quite similar, i.e. the difference between these series is within a few percentage points (~~Fig.6).~~Table 4 and Table 5). There was no need ~~for reevaluation of~~to re-evaluate the KS616 data for the period 2014−2023 ~~as shown by the comparisons~~because they agreed well with the BS64 data (Fig.3 and Fig.~~5~~5).

~~Statistical~~Regression models trained on the KZ616 data for the period 2014−2023 allowed the data to be reconstructed from the beginning of ~~UV~~UVR observations at Belsk. These reconstructed series allowed

independent examination of the pattern of interannual variability (which was unexpectedly large before 1985) and trends in the erythemal annual and summer RE. The ~~statistical~~regression models generally mimic the observed long-term variability in the ~~reevaluated~~re-evaluated daily erythemal exposures. The statistically significant trend of ~6 % per decade with a standard error of ~1 % per decade for the period 1976−2005 can be calculated (for both erythemal annual and summer RE) by averaging trends from the sample of seven versions of trend estimates from ~~reevaluated~~re-evaluated and reconstructed data~~.~~ (Table 7). All individual trend values are within the range of the mean trend ±2 standard error (i.e. there is no outlier in this trend sample).

The standard errors for the individual trend estimates are in the range of 1-1.5% per decade, i.e. quite close to the standard error of the averaged trend derived from the trend sample. This supports the robustness of the trend estimates in annual and summer RE for the 1976−2005 parts of the Belsk time series. In addition, it also appears that the ~~very different calibration~~correction methods applied to the 1976–2013 raw ~~UV~~UVR data, based on the comparisons of clear-sky erythemal DRE (CC1 method) and noon UVI (CC2 method), lead to differences in the individual 1976−2005 trend estimates of about 1 % per decade (see Table ~~6~~7 for the trend differences between pairs of OBS_F, Mod2 and Mod3 calculated with the CC1 and CC2 correction applied to the raw time series).

We found that ~~Mod1 could provide reasonable~~ our DRE estimates ~~of DRE~~ for all biological effects considered (erythema, vitamin D_3 and psoriasis~~), i.e.~~) were close to those obtained from the Brewer's spectra with a bias of ~~less than 2~~ ~ −1 % and a standard deviation of ~ 9 % (Table A1) for the part of the year when ~~UV radiation~~UVR is of particular interest, when the midday SZA is less than 45° (i.e. below the shadow length), according to the so-called shadow rule for protection against high ~~UV~~UVR (Downham, 1998).

Krzyścin et al. (2011) found a trend of 5.6 % ± 0.9 % (1σ) per decade in the erythemal annual RE for the period 1976−2008. This is in good agreement with the present trend estimate, regardless of the very different ~~calibration~~correction methods used. The correction of the SL501 A data carried out in 2011 was based on simultaneous measurements with KZ616 for the period 2008−2009 and further corrections for the instrument ageing using TUV cloudless sky simulations.

Similar trend estimates for erythemal radiation can be inferred from the reconstructed erythemal time series for the Moscow region based on the ~~UV~~UVR measurements by the broadband (300−380 nm) radiometer (Chubarova et al., 2018) and the statistically reconstructed erythemal radiation series for Hradec Kralowe (Čížková et al., 2018). For the Moscow region, the authors reported a statistically significant positive trend of more than 5 % per decade for the period 1979-2015. Volpert and Chubarowa (2021) revealed the decadal trend in the reconstructed erythemal UV irradiance over the Moscow region for the warm season (May−September) of 5.1 % ± 1.1 % per decade in the period 1979−2016. Estimates from the smoothed pattern of annual erythemal exposures taken from Fig. 2c by Čížková et al. (2018) for 1976 (~1.20 kJ m^{-2} for the annual mean of erythemal daily RE) and 2005 (~1.40 kJ m^{-2}) give a trend of ~5% per decade for the period 1976−2004. From around 2005, both time series show a levelling off. Trends calculated here from the RE time series for other biological effects (previtamin D_3 synthesis and psoriasis lesion clearance), using an approach analogous to that used for the erythema data, show very similar trends.

5 Code and data availability

All data have been published as free access TXT files and are made available through PANGEA repository at https://doi.org/10.1594/PANGAEA.972139 (Krzyścin et al., 2024) and IG PAS Data Portal repository: https://doi.org/10.25171/InstGeoph_PAS_IGData_Biologically_Effective_Solar_Radiation_Belsk_1976_2023 (Krzyścin, 2024). ERA5 data are publicly accessible at https://cds.climate.copernicus.eu/datasets/reanalysis-era5-single-levels?tab=overview (ERA5, ~~2024~~2025). MERRA-2 data are accessible at https://doi.org/10.5067/Q9QMY5PBNV1T (GMAO, ~~2024~~2025). Coefficients of the linear regression are calculated by Matlab function (Matlab R2018a) – *fitlm(x,y)*.

6 Conclusions

It is widely accepted that the use of overlapping measurement series from different instruments increases the reliability of results obtained from single time series analyses. Consequently, the inclusion of at least two different time series for analyses of the variability of a selected quantity over the entire measurement period is also beneficial for assessing data quality and establishing confidence in the results obtained. This is illustrated by the current data archived in the PANGEA (Krzyścin et al., 2024) and IG ~~PAN~~PAS Data Portal (Krzyścin, 2024). The daily characteristics of BE radiation at Belsk allow the elaboration of scenarios of human outdoor activities to obtain maximum health benefits from sunbathing while minimising the risk of erythemal overexposure. The long-term variability of erythemal radiation calculated for Belsk corresponds to that previously recorded at distant stations in central/eastern Europe, making these scenarios applicable to wider areas.

Appendix A

Table A1 presents descriptive statistics (defined in Sect. 2.4) of the relative differences between biologically effective DRE measured by the ~~BS64~~KZ616 and the ~~KZ616~~BS64, $100\%(RE_{EFF,\,\sout{BS64}KZ616} - RE_{EFF,\,\sout{KZ616}BS64})/RE_{EFF,BR64}$. The vitamin D_3 (VitD) and antipsoriatic (Psor) RE were reconstructed from the erythemal (Eryt) RE (Sect. 2.3.3), but the Brewer RE values were calculated using the daily integral of the measured spectral irradiance weighted by the action spectra (Fig.1).

Table A1. Descriptive statistics of the 2014-2023 relative differences between the daily biologically effective radiant exposure with the ~~Brewer spectrophotometer #064 and the~~ Kipp & Zonen erythema ~~biometer~~radiometer (UV-S-AE-T #30616) ~~at Belsk~~and the Brewer spectrophotometer #064 in percent of the Brewer data for the different midday SZA ranges (SZA_N~~) used in the Mod1 setup.~~).

Statistics	$SZA_N<45^{oo}$			SZA_N [45º, 60º]			$SZA_N \geq 60^{o}$			All SZA_N		
	Eryt	VitD	Psor	Eryt	VitD	Psor	Eryt	VitD	Psor	Eryt	VitD	Psor
~~MRE~~MRD	–0.6	–1.5	–0.7	–2.5	–6.6	–3.3	–1.7	–13.2	–1.7	–1.4	–6.8	–1.6
~~MAE~~MAD	5.3	6.0	5.6	4.9	7.9	5.4	6.8	14.7	7.0	5.8	9.6	6.1
~~RMSE%~~RMSD	8.7	9.2	9.0	7.2	10.0	7.8	10.0	16.3	10.3	8.9	12.4	9.3
SD~~%~~	8.7	9.1	9.0	6.8	7.6	7.1	9.9	9.5	10.2	8.8	10.4	9.1

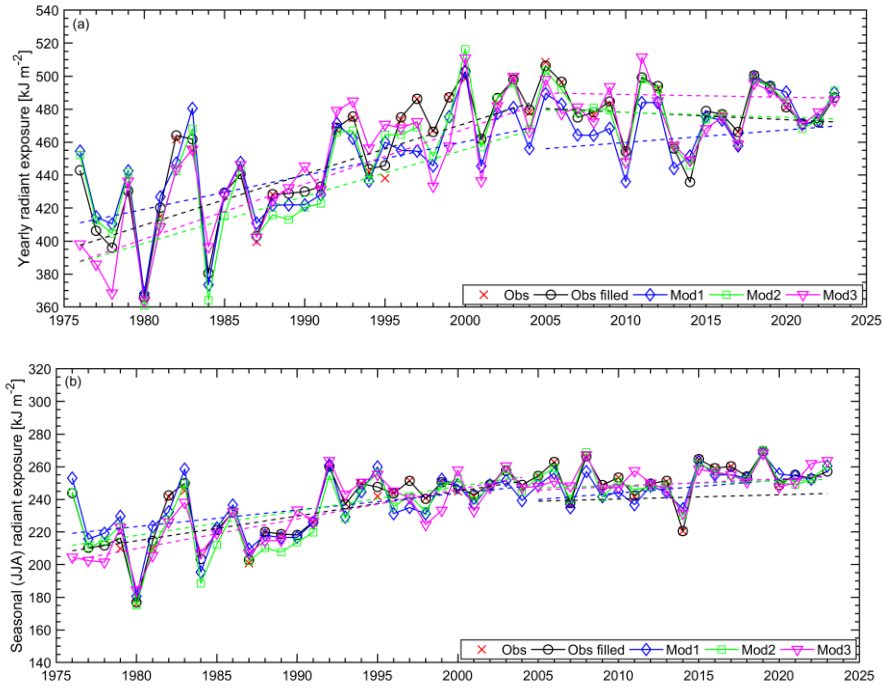

Figure A1. Same as Fig.8, but for the ~~reevaluated~~re-evaluated observations with the CC2 correction coefficients.

Authors contributions. Conceptualisation, JK and AC; methodology, JK, AC, JJ, PS, and BR; validation, AC and IP; visualisation, AC; writing (original draft preparation), JK and AC; writing (review and editing), JK, AC, PS, and IP; funding acquisition, JK and JJ. All authors have read and agreed to the published version of the paper.

Competing interests. The contact author has declared that none of the authors has any competing interests.

Acknowledgments. This work was partially financially by the Chief Inspectorate of Environment Protection, contract number GIOŚ/31/2023/DMŚ/NFOŚ.

References

~~**References**~~

AERONET: Aerosol Robotic Network: https://aeronet.gsfc.nasa.gov/, last access: ~~30 December 2024~~15 April 2025.

Berger, D. S.: The sunburning ultraviolet meter: design and performance, Photochem. Photobiol., 24, 587–593, 1976.

Blumthaler, M., Ambach, W., Morys, M., and Slomka J.: Comparison of Robertson-Berger UV Meters From Innsbruck and Belsk, Publs. Inst. Geophys. Pol. Acad. Sc., D-32 (230), 1989.

Borkowski, J. L.: Reevaluation of series of solar UV-B radiation data, Publs. Inst. Geophys. Pol. Acad. Sc., D-48, 291, 81–89, 1998.

729 Borkowski, J. L.: Homogenization of the Belsk UV-B series (1976–1997) and trend analysis, J. Geophys. Res.,
730 105(D4), 4873–4878, https://doi.org/10.1029/1999JD900500, 2000.

731 Borkowski, J.L.: Modelling of UV radiation at different time scales, Ann. Geophys., 26, 3, 441–446,
732 https://doi.org/10.5194/angeo-26-441-2008, 2008.

733 ~~Blumthaler, M., Ambach, W., Morys, M., and Slomka J.: Comparison of Robertson Berger UV Meters From~~
734 ~~Innsbruck and Belsk, Publs. Inst. Geophys. Pol. Acad. Sc., D-32 (230), 1989.~~

735 Chubachi, S.: Preliminary result of ozone observations at Syowa Station from February, 1982 to January, 1983,
736 Mem. NatI. Inst. Polar Res., Spec. Issue (Jpn), 34, 13–20, 1984.

737 Chubarova, N. Y., and Nezval', Y. I.: Thirty year variability of UV irradiance in Moscow, J. Geophys. Res., 105,
738 12529–12539, https://doi.org/10.1029/1999JD901192, 2000.

739 Chubarova, N. E., Pastukhova, A. S., Galin, V. Y., and Smyshlyaev, S. P.: Long-Term Variability of UV Irradiance
740 in the Moscow Region according to Measurement and Modeling Data, Izv. Atmos. Ocean. Phys., 54, 139–146,
741 https://doi.org/10.1134/S0001433818020056, 2018.

742 CIE 174:2006: Commission Internationale de l'Eclairage. Action Spectrum for the Production of Previtamin D3
743 in Human Skin. CIE: Vienna, Austria, pp.1–16, 2006.

744 CIE 17166:2019(E): Commission Internationale de l'Eclairage. Erythema Reference Action Spectrum and
745 Standard Erythema Dose. CIE, Vienna, Austria, pp.1-5, 2019.

746 Čížková, K., Láska, K., Metelka, L., and Staněk, M.: Reconstruction and analysis of erythemal UV radiation time
747 series from Hradec Králové (Czech Republic) over the past 50 years, Atmos. Chem. Phys., 18, 1805–1818,
748 https://doi.org/10.5194/acp-18-1805-2018, 2018.

749 Cleveland, W. S.: Robust Locally Weighted Regression and Smoothing Scatterplots, J. Am. Stat. Assoc., 74 (368),
750 829–836, https://doi.org/10.1080/01621459.1979.10481038, 1979.

751 Czerwińska, A., and Krzyścin, J.: Measurements of biologically effective solar radiation using erythemal weighted
752 broadband meters, Photochem. Photobiol. Sci., 23, 479–492, https://doi.org/10.1007/s43630-023-00532-z, 2024a.

753 Czerwińska, A., and Krzyścin, J.: Modeling of Biologically Effective Daily Radiant Exposures over Europe from
754 Space Using SEVIRI Measurements and MERRA-2 Reanalysis, Remote Sens., 16— (20), 3797,
755 https://doi.org/10.3390/rs16203797, 2024b.

756 Dave, J.V. and Halpern, P.; Effect of changes in ozone amount on the ultraviolet radiation received at sea level of
757 a model atmosphere, Atmos. Environ. 10(7), 547-555, https://doi.org/10.1016/0004-6981(76)90181-5, 1976.

758 den Outer, P. N., Slaper, H., Kaurola, J., Lindfors, A., Kazantzidis, A., Bais, A. F., Feister, U., Junk, J., Janouch,
759 M., and Josefsson, W.: Reconstructing of erythemal ultraviolet radiation levels in Europe for the past 4 decades,
760 J. Geophys. Res., 115, D10102, https://doi.org/10.1029/2009JD012827, 2010.

761 Downham, T. F. 2nd: The shadow rule: a simple method for sun protection, South Med J., 91 (7), 619–623, 1998.

ERA5: ERA5 hourly data on single levels from 1940 to present, https://cds.climate.copernicus.eu/datasets/reanalysis-era5-single-levels?tab=overview, last access ~~30 December 2024.~~15 April 2025.

Farman, J., Gardiner, B., and Shanklin, J.: Large losses of total ozone in Antarctica reveal seasonal ClO_x/NO_x interaction, Nature, 315, 207–210, https://doi.org/10.1038/315207a0, 1985.

Giovanni: The Bridge Between Data and Science v 4.40: https://giovanni.gsfc.nasa.gov/giovanni/, last access ~~30 December 2024~~15 April 2025.

GMAO: Global Modeling and Assimilation Office, MERRA-2 tavg1_2d_rad_Nx: 2d,1-Hourly, Time-Averaged, Single-Level, Assimilation, Radiation Diagnostics V5.12.4, Greenbelt, MD, USA, Goddard Earth Sciences Data and Information Services Center (GES DISC), https://doi.org/10.5067/Q9QMY5PBNV1T, last access ~~30 December 2024~~15 April 2025.

Gröbner, J., Hülsen, G., Vuilleumier, L., Blumthaler, M., Vilaplana, J. M., Walker, D., and Gill, J. E.: Report of the PMOD/WRC-COST Calibration and Intercomparison of Erythemal Radiometers. Physical Meteorological Observatory Davos World Radiation Center (PMOD-WRC) Pub., 119 pp, Brussels, Belgium, 2009.

Hülsen, G., and Gröbner, J.: Characterization and calibration of ultraviolet broadband radiometers measuring erythemally weighted irradiance, Appl. Opt., 46 (23), 5877–5886, https:/doi.org/10.1364/AO.46.005877, 2007.

Koepke, P., De Backer, H., Bais, A., Curylo, A., Eerme, K., Feister, U., Johnsen, B., Junk, J., Kazantzidis, A., Krzyścin, J., Lindfors, A., Olseth, J. A., den Outer, P., Pribullova, A., Schmalwieser, A. W., Slaper, H., Staiger, H., Verdebout, J., Vuilleumier, L., and Weihs, P.: Modelling solar UV radiation in the past: Comparison of algorithms and input data, Proc. SPIE, 6362, Remote Sensing of Clouds and the Atmosphere XI, 636215, https://doi.org/10.1117/12.687682, 2006.

Koskela T., Taalas, P., and Leszczynski, K.: Correction method for Robertson Berger type ultraviolet radiometer data, Proc. 8th Conference on Atmospheric Radiation, Nashville, Tennessee, USA, 161–163, 1994.

Krzyścin, J. W.: Biologically effective solar radiation (daily radiant exposure and irradiance at noon) at Belsk from 1 January 1976 to 31 December 2023 based on homogenised measurements with broadband radiometers, IG PAS [dataset], https://doi.org/10.25171/InstGeoph_PAS_IGData_Biologically_Effective_Solar_Radiation_Belsk_1976_2023, 2024.

Krzyścin, J. W., and Puchalski, S.: Aerosol impact on the surface UV radiation from the ground-based measurements taken at Belsk, Poland, 1980–1996, J. Geophys. Res., 103 (D13), 16175–16181, 1998.

Krzyścin, J. W., Sobolewski, P. S., Jarosławski, J., Podgórski, J., and Rajewska-Więch, B.: Erythemal UV observations at Belsk, Poland, in the period 1976–2008: Data homogenization, climatology, and trends, Acta Geophys., 59, 155–182, https://doi.org/10.2478/s11600-010-0036-3, 2011.

Krzyścin, J. W., Jarosławski, J., Rajewska-Więch, B., Sobolewski, P. S., Narbutt, J., Lesiak, A., and Pawlaczyk, M.: Effectiveness of heliotherapy for psoriasis clearance in low and mid-latitudinal regions: A theoretical approach, J. Photochem. Photobiol. B Biol., 115, 35–41, https://doi.org/10.1016/j.jphotobiol.2012.06.008, 2012.

Krzyścin, J. W., Sobolewski, P., Czerwińska, A., Rajewska-Więch, B., Jarosławski, J.: Biologically weighted daily radiant exposure for erythema appearance, previtamin D_3 synthesis and clearing of psoriatic lesions from erythema biometers at Belsk, Poland, for the period 1976-2023, PANGAEA [dataset], https://doi.org/10.1594/PANGAEA.972139, 2024.

Leszczynski, K., Jokela, K., Ylianttila, L., Visuri, R., Blumthaler, M.: Erythemally Weighted Radiometers in Solar UV Monitoring: Results from the WMO/STUK Intercomparison, Photochem. Photobiol., 67 (2), 212–221, https://doi.org/10.1111/j.1751-1097.1998.tb05189.x, 1998.

~~Liu, B. Y., and Jordan, R. C.: The interrelationship and characteristic distribution of direct, diffuse, and total solar radiation, Sol. Energy, 4 (3), 1–19, https://doi.org/10.1016/0038-092X(60)90062-1, 1960.~~

Molina, M. J., and Rowland, F. S.: Stratospheric sink for chlorofluoromethanes: chlorine atom-catalyzed destruction of ozone, Nature, 249, 810–812, https://doi.org/10.1038/249810a0, 1974.

NDACC, Network for the Detection of Atmospheric Composition Change, https://www-air.larc.nasa.gov/missions/ndacc/, last access: 15 April 2025.

Neale, R. E., Lucas, R. M., Byrne, S. N., Hollestein, L., Rhodes, L. E., Yazar, S., Young, A. R., Berwick, M., Ireland, R. A., and Olsen, C. M.: The effects of exposure to solar radiation on human health, Photochem. Photobiol. Sci., 22, 1011–1047, https://doi.org/10.1007/s43630-023-00375-8, 2023.

Posyniak, M., Szkop, A., Pietruczuk, A., Podgórski J., and Krzyścin, J.: The long-term (1964-2014) variability of aerosol optical thickness and its impact on solar irradiance based on the data taken at Belsk, Poland, Acta Geophys., 64, 1858–1874, https://doi.org/10.1515/acgeo-2016-0026, 2016.

Puchalski, S.: Preliminary results of the comparison of Robertson-Berger meter with the UV-Biometer MOD 501A, version 3, produced by Solar Light Co., Publs. Inst. Geophys. Pol. Acad. Sc. D-42(269), 113–115, 1995.

Rieder, H. E., Holawe, F., Simic, S., Blumthaler, M., Krzyścin, J. W., Wagner, J. E., Schmalwieser, A. W., and Weihs, P.: Reconstruction of erythemal UV-doses for two stations in Austria: a comparison between alpine and urban regions, Atmos. Chem. Phys., 8, 6309–6323, https://doi.org/10.5194/acp-8-6309-2008, 2008.

Schmalwieser, A. W., Eschenbacher, S., and Schreder, J.: UV-Biometer - The usage of erythemal weighted broadband meters for other biological effects, J. Photochem. Photobiol. B Biol., 230, 112442, https://doi.org/10.1016/j.jphotobiol.2022.112442, 2022.

Scotto, J., Cotton, G., Urbach, F., Berger, D., and Fears, T.: Biologically effective ultraviolet radiation: surface measurements in the United States, 1974 to 1985, Science, 239 (4841), 762–764, https://doi.org/10.1126/SCIENCE.3340857, 1988.

Słomka, J., and Słomka, K.: Comparison of Robertson-Berger ultraviolet meter counts with the UVB and Uver radiation inflow determined from Dave-Halpern's model, Publs. Inst. Geophys. Pol. Acad. Sc., D-22 (189), 133–143, 1985.

Słomka, J., and Słomka, K.: Biologically active solar UV radiation at Belsk in the years 1976-1992, Publs. Inst. Geophys. Pol. Acad. Sc., D-40 (263), 71–81, 1993.

TUV: Tropospheric Ultraviolet and Visible (TUV) Radiation Model: https://www2.acom.ucar.edu/modeling/tropospheric-ultraviolet-and-visible-tuv-radiation-model, last access ~~30 December 2024~~15 April 2025.

Volpert, E.V., and Chubarova, N.E.: Long-term changes in solar radiation in Northern Eurasia during the warm season according to measurements and reconstruction model. Russ. Meteorol. Hydro+, 46(8), 507–518, https://doi.org/10.3103/S1068373921080021, 2021.

Weatherhead, E. C., Reinsel, G. C., Tiao, G. C., Meng, X., Choi, D., Cheang, W., Keller, T., DeLuisi, J., Wuebbles, D. J., Kerr, J. B., Miller, A. J., Oltmans, S. J., and Frederick, J. E.: Factors affecting the detection of trends: Statistical considerations and applications to environmental data, J. Geophys. Res., 103 (D14), 17149–17161, https://doi.org/10.1029/98JD00995, 1998.

WMO: World Meteorological Organization, UNEP, Report of the Meeting of Experts on UV-B Monitoring and Research, GORMP-No. 03, WMO, Geneva, Switzerland, 1977.

WOUDC: World Ozone and Ultraviolet Radiation Data Centre, https://woudc.org/data.php, last access 15 April 2025.